Article

Two-Photon Uncaging with Fluorescence Reporting: Evaluation of the *o*-Hydroxycinnamic Platform

Nathalie Gagey, Pierre Neveu, Chouaha Benbrahim, Bernard Goetz, Isabelle Aujard, Jean-Bernard Baudin, and Ludovic Jullien

J. Am. Chem. Soc., **2007**, 129 (32), 9986-9998• DOI: 10.1021/ja0722022 • Publication Date (Web): 21 July 2007

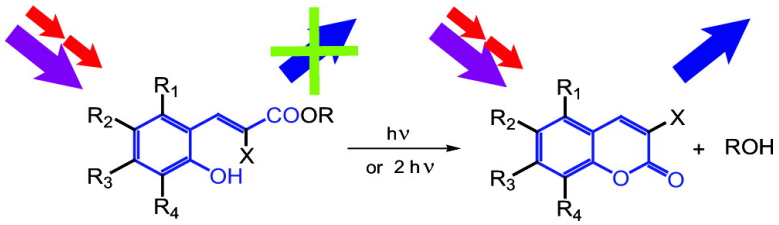

More About This Article

Additional resources and features associated with this article are available within the HTML version:

- Supporting Information
- Links to the 1 articles that cite this article, as of the time of this article download
- Access to high resolution figures
- Links to articles and content related to this article
- Copyright permission to reproduce figures and/or text from this article

View the Full Text HTML

J|A|C|S
ARTICLES
Published on Web 07/21/2007

Two-Photon Uncaging with Fluorescence Reporting: Evaluation of the *o*-Hydroxycinnamic Platform

Nathalie Gagey,[†] Pierre Neveu,[†,‡] Chouaha Benbrahim,[†] Bernard Goetz,[#] Isabelle Aujard,[†] Jean-Bernard Baudin,[†] and Ludovic Jullien*[,†]

Contribution from the École Normale Supérieure, Département de Chimie, UMR CNRS-ENS-Université Paris 6 8640 PASTEUR, 24, rue Lhomond, 75231 Paris Cedex 05, France, École Normale Supérieure, Laboratoire de Physique Statistique, UMR CNRS-ENS-Université Paris 6 and Paris 7 8550, 24, rue Lhomond, 75231 Paris Cedex 05, France, and École Normale Supérieure, Département de Chimie, UMR CNRS-ENS-Université Paris 6 8642; 24, rue Lhomond, 75231 Paris Cedex 05, France

Received March 29, 2007; E-mail: ludovic.jullien@ens.fr

Abstract: This paper evaluates the *o*-hydroxycinnamic platform for designing efficient caging groups with fluorescence reporting upon one- and two-photon excitation. The model cinnamates are easily prepared in one step by coupling commercial or readily available synthons. They exhibit a large one-photon absorption that can be tuned in the near-UV range. Uncaging after one-photon excitation was investigated by ^{1}H NMR, UV−vis absorption, and steady-state fluorescence emission. In the whole investigated series, the caged substrate is quantitatively released upon photolysis. At the same time, uncaging releases a strongly fluorescent coproduct that can be used as a reporter for quantitative substrate delivery. The quantum yield of double bond photoisomerization leading to uncaging after one-photon absorption mostly lies in the 10% range. Taking advantage of the favorable photophysical properties of the uncaging coproduct, we use a series of techniques based on fluorescence emission to measure the action uncaging cross sections with two-photon excitation of the present cinnamates. Exhibiting values in the 1−10 GM range at 750 nm, they satisfactorily compare with the most efficient caging groups reported to date. Noticeably, the uncaging behavior with two-photon excitation is retained in vivo as suggested by the results observed in living zebrafish embryos. Reliable structure property relationships were extracted from analysis of the present collected data. In particular, the careful kinetic analysis allows us to discuss the relevance of the *o*-hydroxycinnamic platform for diverse caging applications with one- and two-photon excitation.

Introduction

The spatio-temporal delivery pattern of precise given amounts of chemicals is of major importance in chemistry and biology. Syringes have been used to achieve this goal at the microscopic level. However such microinjections, by their invasive nature, are not appropriate if the targeted organism has to remain intact. Given the excellent intrinsic localization in two-photon excitation,[1] photoactivation has been envisioned to provide an attractive noninvasive alternative: the "optical microsyringe''.[2−5] In the corresponding approach, a focused light pulse is used to release within an organism perfused with a solution of a biologically nonactive precursor the desired chemical after two-photon photoactivation (or uncaging).[6]

A large enough two-photon action uncaging cross section is a key factor to satisfactorily implement the preceding two-photon photoactivation strategy in sensitive samples. In fact, the cross section should be as large as possible to reduce the illumination duration and power needed to release a given amount of effector without generating detrimental effects. For instance, it was claimed to have to exceed 0.1 or 10 Goeppert−Mayer (GM; 1 GM = 10^{-50} cm^{4}s/photon) for biological applications.[3,7] In fact, the 1 GM range has already been reached,[3,8,9] and the corresponding caging groups have been successfully used in biological systems. Nevertheless the improvement of the efficiency of a photolabile protecting group upon two-photon excitation remains difficult, and it is therefore useful to gain reliable structure property relationships. Indeed we still lack general rules to predict the cross section for two-

[†] UMR CNRS-ENS-Université Paris 6 8640 PASTEUR.
[‡] UMR CNRS-ENS-Université Paris 6 and Paris 7 8550.
[#] UMR CNRS-ENS-Université Paris 6 8642.

(1) Xu, C.; Zipfel, W.; Shear, J. B.; Williams, R. M.; Webb, W. W. *Proc. Natl. Acad. Sci. U.S.A.* **1996**, *93*, 10763−10768.
(2) Cambridge, S. B.; Davis, R. L.; Minden, J. S. *Science* **1997**, *277*, 825−828.
(3) Furuta, T.; Wang, S. S. H.; Dantzker, J. L.; Dore, T. M.; Bybee, W. J.; Callaway, E. M.; Denk, W.; Tsien, R. Y. *Proc. Nat. Acad. Sci. U.S.A.*, **1999**, *96*, 1193−1200.
(4) Ando, H.; Furuta, T.; Tsien, R. Y.; Okamoto, H. *Nat. Genet.* **2001**, *28*, 317−325.
(5) Momotake, A.; Lindegger, N.; Niggli, E.; Barsotti, R. J.; Ellis-Davies, G. C. R. *Nat. Methods* **2006**, *3*, 35−40.
(6) Mayer, G.; Heckel, A. *Angew. Chem., Int. Ed.*, **2006**, *45*, 4900−4921.
(7) Kiskin, N.; Chillingworth, R.; McCray, J. A.; Piston, D.; Ogden, D. *Eur. Biophys. J.* **2002**, 30, 588−604.
(8) Lu, M.; Fedoryak, O. D.; Moister, B. R.; Dore, T. M. *Org. Lett.* **2003**, *5*, 2119−2122.
(9) Gagey, N.; Neveu, P.; Jullien, L. *Angew. Chem., Intl. Ed.* **2007**, *46*, 2467−2469.

10.1021/ja0722022 CCC: $37.00

photon absorption of a chromophore from its structure. In addition, it is not obvious to predict the quantum yield of uncaging after two-photon excitation, even when the corresponding quantum yield of uncaging after one-photon excitation is known. Indeed the mechanism leading to uncaging could depend on the excitation mode.

Another important issue is the quantification of delivery upon uncaging, when one is interested to reach a critical molecule concentration to induce a specific activity. First, calibration of the laser power can be made difficult in complex systems (e.g., a living organism) because of the uncertainties associated to many unknown medium characteristics regarding volume, viscosity, optical homogeneity, etc. Second, the system response can strongly depend on the amount of uncaged substrate (e.g., biological response resulting from the interaction between a photoreleased ligand and its biological target). An elegant way to address this quantification task relies on the simultaneous release of a fluorescent reporter and the desired caged substrate from the same nonfluorescent caged precursor. Quantitative analysis could be then simply obtained from analyzing the increase of fluorescence emission after or better during uncaging at the targeted site. Whereas numerous caging groups have been continuously introduced with the goal to improve their photophysical and photochemical characteristics,[10−12] uncaging quantification using an optical method has attracted little attention. Indeed, in most cases, the caged substrate and the coproduct from the photolabile moiety after uncaging exhibit similar brightnesses. From the latter point of view, the coumaryl photolabile protecting group was shown to be satisfactory in several occurrences.[13] Nevertheless the absence of fluorescence emission in the caged substrate was not intrinsic in the reported systems but was associated to the quenching of the reporter fluorescence by the substrate moiety: Hence, beyond the restriction for caging acidic substrates, the coumaryl photolabile protecting group lacks of generality for the reporting purpose.

The preceding considerations led us to consider with high interest the *o*-hydroxycinnamic platform that was introduced to cage alcohols and amines by Porter et al.[14−16] In this series, the primary event leading to uncaging is light absorption by the cinnamic backbone that belongs to the extensively investigated series of donor−acceptor ethylenic systems. In the context of two-photon excitation, the wavelength maximum and the value of the cross section for two-photon absorption of such donor−acceptor ethylenic systems can be now reasonably predicted from the molecular structure.[17,18] Their photophysical behavior is also satisfactorily established, in particular the competition between fluorescence emission and isomerization in the excited state.[19−21] In addition, the mechanism and kinetics of the thermal reactions involved in the formation of the coumarin coproduct accompanying the release of the caged substrate are already well-documented.[22,23] Eventually the reported cinnamates intrinsically do not fluoresce, in marked contrast with the photoreleased coumarin coproduct. The latter behavior is here particularly attractive in relation to the intended purpose of having a fluorescent reporter upon uncaging.

The present paper examines the *o*-hydroxycinnamic platform to tailor efficient photolabile protecting groups that exhibit large two-photon uncaging action cross sections and that release strongly fluorescent coproducts upon uncaging. The first section deals with the design and the syntheses of two series of model *o*-hydroxycinnamate that differ by the substitution pattern of the double bond. The second section evaluates the present series of photolabile protecting groups with one-photon excitation. After an initial screen to identify the most promising substitution patterns, we characterize the one-photon absorption properties of the compounds, then we determine the uncaging mechanism, the corresponding kinetics associated to the photochemical step and the subsequent thermal step, and the uncaging action cross section with one-photon excitation. In the third section, we determine the uncaging action cross sections with two-photon excitation of the most promising caging groups in the investigated series. Then we demonstrate the relevance of the *o*-hydroxy platform for biological applications by investigating two-photon uncaging in a zebrafish embryo. Section 4 is devoted to the discussion. In particular, we show that the choice of the "best'' *o*-hydroxycinnamic caging moiety is not intrinsic but depends on the considered application and on the experimental constraints. Concluding remarks are eventually given in section 5.

Design and syntheses

Our investigation of the *o*-hydroxycinnamic platform for uncaging applications starts from the original design of Porter (Figure 1).[24]

Retaining a same cinnamate series leading to alcohol release upon uncaging, we aimed at studying the significance of different structural parameters to optimize the photorelease efficiency. As suggested in the introduction, we were especially interested in establishing structure−property relationships to improve the uncaging action cross sections with two-photon excitation as well as the fluorescence reporting features. Nevertheless, we also considered other aspects such as thermal

(10) Pillai, V. N. R. *Synthesis* **1980**, 1−26.
(11) Bochet, C. G. *J. Chem. Soc., Perkin Trans.* **2002**, *1*, 125−142.
(12) Pelliccioli, A. P.; Wirz, J. *Photochem. Photobiol. Sci.* **2002**, 1, 441−458.
(13) Hagen, V.; Frings, S.; Bendig, J.; Lorenz, D.; Wiesner, B.; Kaupp, U. B. *Angew. Chem., Intl. Ed.* **2002**, *41*, 3625−3628.
(14) Turner, A. D.; Pizzo, S. V.; Rozakis, G.; Porter, N. A. *J. Am. Chem. Soc.* **1988**, *110*, 244−250.
(15) Wang, B. H.; Zheng, A. *Chem. Pharm. Bull.* **1997**, *45*, 715−718.
(16) Li, H.; Yang, J. H.; Porter, N. A. *J. Photochem. Photobiol. A* **2005**, 169, 289−297.
(17) Xu, C.; Webb, W. W. *J. Opt. Soc. Am. B* **1996**, *13*, 481−491.
(18) Cogné-Laage, E.; Allemand, J. F.; Ruel, O.; Baudin, J. B.; Croquette, V.; Blanchard-Desce, M.; Jullien, L. *Chem.−Eur. J.* **2004**, *10*, 1445−1455.
(19) Dauben, W. G.; Salem, L.; Turro, N. J. *Acc. Chem. Res.* **1975**, *8*, 41−54.
(20) Burghardt, I.; Cederbaum, L. S.; Hynes, J. T. *Faraday Discuss.* **2004**, *127*, 395−411.
(21) Burghardt, I.; Hynes, J. T. *J. Phys. Chem. A* **2006**, 110, 11411−11423.
(22) Hershfield, R.; Schmir, G. L. *J. Am. Chem. Soc.* **1973**, *95*, 7359−7369.
(23) Hershfield, R.; Schmir, G. L. *J. Am. Chem. Soc.* **1973**, *95*, 8032−8040.
(24) In the course of the present work, we also considered relying on the *o*-aminocinnamic platform for uncaging applications as reported by Porter in ref 16. Indeed we expected that this series should be particularly favorable to get large k_2 constants because of the lower electronegativity of the nitrogen atom with regard to the oxygen one. Thus we synthesized the 3-(6-amino-benzo(1,3)dioxo-5-yl)-acrylic acid ethyl ester in two steps by condensing the 1-carboxymethyliden triphenyl phosphorane on 6-amino-3,4-methylenedioxybenzaldehyde that was obtained from Fe/HCl reduction of 6-nitro-3,4-methylenedioxybenzaldehyde in a mixture of acetic acid, ethanol, and water. 3-(6-Amino-benzo(1,3)dioxo-5-yl)-acrylic acid ethyl ester exhibits satisfactory absorption properties: in Tris (pH = 7) 20 mM NaCl 100 mM buffer/acetonitrile 1/1 (v/v), $\epsilon_E(\lambda_E^{(1)}) = 13 \times 10^3\ M^{-1}\ cm^{-1}$ at 385 nm. The quinolone resulting from uncaging is also reasonably fluorescent ($\lambda_F^{(1)} = 390$ nm; $\Phi_F^{(1)} = 7\%$), although less than the coumarins obtained from the present *o*-hydroxycinnamic derivatives. Unfortunately, whereas k_2 was indeed so large that we were unable to measure it (subsecond time scale; see ref 16), k_1 was found to be extremely low ($1.7\ 10^{-5}\ s^{-1}$ with $I_0(\lambda_{exc}^1) = 2.1\ 10^{-7}$ einstein min^{-1}; k_1 is here typically two orders of magnitude smaller than in the *o*-hydroxycinnamate series; see Table 1S) forbidding to rely on the *o*-aminocinnamic platform to develop an efficient series of photolabile protecting groups for two-photon uncaging applications.

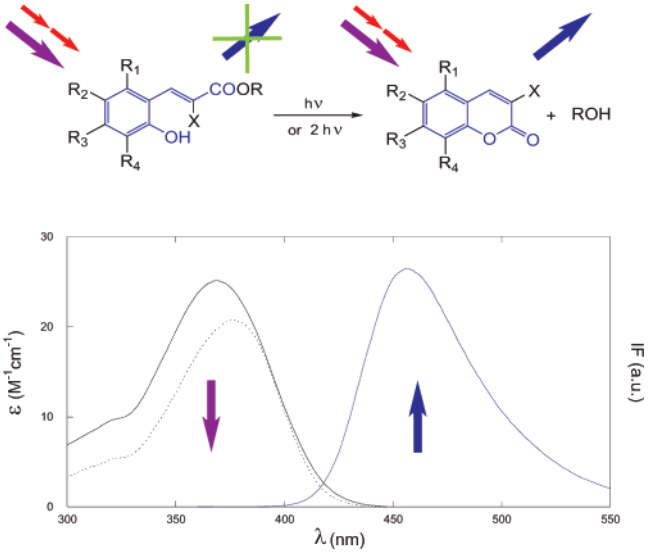

Figure 1. The *o*-hydroxycinnamic platform to illustrate uncaging with fluorescence reporting. The intrinsically nonfluorescent cinnamate of the alcohol substrate **ROH** is illuminated in a wavelength range where it absorbs light (violet and red arrows with one- and two-photon excitation, respectively). Light absorption initiates a series of photochemical and thermal processes in the *o*-hydroxycinnamate backbone leading to release the **ROH** substrate together with the fluorescent coumarin **F** coproduct in a one-to-one stoichiometric ratio. As the starting cinnamate and the coumarin coproduct absorb light in the same wavelength range (black solid and dotted lines, respectively), the **F** coumarin continuously emits fluorescence (blue solid line) upon uncaging and its fluorescence intensity reports on the uncaging extent. The absorption and emission properties of the cinnamate **Ec** at 293 K in Tris(pH = 7) 20 mM NaCl 100 mM buffer/acetonitrile 1/1 (v/v) are used for a purpose of illustration.

Chart 1. Structures of the **E′** Series of Photolabile Protecting Groups Investigated in the Present Study

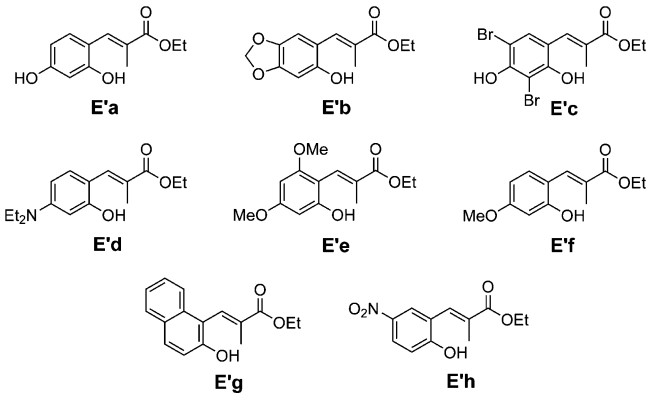

stability, water solubility, kinetics of substrate release, etc., which can prove to be crucial for biological applications.

To examine the role of the substitution pattern of the double bond, we synthesized two closely related series of cinnamates sharing the same (*E*) stereochemistry. Chart 1 and Chart 2 displays the two different **E′** and **E** series that were evaluated during the present study.

The **E′** series relies on the original design of Porter: It incorporates a methyl substituent on the trisubstituted double bond. In contrast, the **E** series contains only disubstituted derivatives in which the double bond bears the carboxylate group on one hand and the substituted aromatic moiety on the other hand. Both series are ethyl cinnamate leading to the release of ethanol upon uncaging. The choice of the ethyl moiety was here

Chart 2. Structures of the **E** Series of Photolabile Protecting Groups Investigated in the Present Study

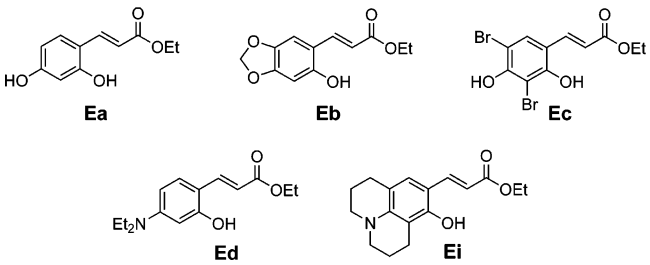

Scheme 1. Syntheses of the Caged Model Alcohols (X = H and X = Me in the **E** and **E′** Series, Respectively)

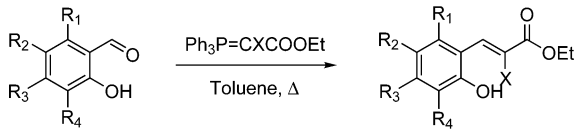

related to its neutrality with regards to the photophysical and photochemical properties of the cinnamate backbone.

In both series, the substitution pattern of the phenyl ring was designed to locate the maximum of two-photon absorption in the 700−900 nm wavelength range that is currently available with the common IR pulsed laser sources. In particular, we grafted several electron-releasing moieties on the phenyl position para to the vinyl carboxylate group. The molecular design was here facilitated by the resulting unsymmetrical donor−acceptor conjugated structure for which the position of the two-photon absorption maximum usually satisfactorily compares with twice the corresponding one of the one-photon absorption.[17,18]

In the present series, the syntheses are short, easy, and rely on commercially available or readily accessible synthons. All the cinnamic esters displayed in Charts 1 and 2 were synthesized with good yields in one step by condensing the substituted salicylaldehydes with the appropriate phosphorane (Scheme 1).[25] It is essential here to pay attention to protecting the reactive medium from light and to accurately controlling heat and time to reduce the formation of the coumarin resulting either from photo- or thermal isomerizations.

Uncaging with One-Photon Excitation. The physicochemical experiments with one-photon excitation were performed stepwise. First, we screened the photophysical and photochemical behavior of the **E′a**−**h** series in aqueous solutions. The purpose was here to evaluate the solubility issue, the wavelength of maximum light absorption with one-photon excitation and the robustness of the photochemical behavior leading to the alcohol release. The results led us to identify (i) the members of the second series **Ea**−**i** by keeping the most promising substituents on the phenyl group of the cinnamate and (ii) appropriate experimental conditions, in particular the solvent, to allow comparisons between the different cinnamates.

Preliminary Screening. In view of possible biological applications, the **E′a**−**h** series has been first tentatively evaluated in aqueous solutions. At that step, its members that did not exhibit enough water solubility at the submillimolar concentrations required for NMR, and UV−vis absorption experiments were dissolved after adding a small amount of cosolvent. The cinnamate solutions were irradiated with one-photon excitation

(25) Porter, N. A.; Thuring, J. W., H. Li *J. Am. Chem. Soc.* **1999**, *121*, 7719−7717.

Table 1. Photophysical and Photochemical Properties of the Investigated (*E*)-Cinnamates That Are Relevant to the Uncaging Process with One- and Two-Photon Excitation[a]

	$10^{-3}\epsilon_E(\lambda_E^{(1)})$ $M^{-1}\,cm^{-1}$ (nm)	$\lambda_F^{(1)}[\Phi_F^{(1)}]$ nm[%]	$\lambda_{exc}^{(1)}$ nm	Q_E/Q_F	$\Phi_{EZ}^{(1)}$ %	$\epsilon_E(\lambda_{exc}^{(1)})\Phi_{EZ}^{(1)}$ $mM^{-1}\,cm^{-1}$	$K_1(\lambda_{exc}^{(1)})$	$k_2, \not{k}_2$ $10^{-3}\,s^{-1}$	$\delta_E(750)\Phi_{EZ}^{(2)}$ GM
Ea	18(331)	452 [40]	350	0.005	9	1.0	0.2	1.6,1.6	*b*
Eb	16(360)	423 [30]	350	*c*	3	0.4	0.2	3.2,4.8	3.8
Ec	25(369)	454 [70]	350	0.025	5	1.2	0.5	2.2,2.2	0.6
Ed	28(378)	475 [60]	360	0.060	2	0.4	0.1	3.7,6.2	2.0
Ei	20(394)	482 [50]	370	0.015	3	0.4	0.1	9.5,9.1	4.7
E′a	17(319)	461 [50]	330	0.070	7	1.0	0.8	10,8	*b*
E′b	14(344)	421 [40]	350	0.050	10	1.3	3.5	30,35	*b*
E′d	31(362)	473 [40]	350	0.050	10	2.7	0.9	12,11	*b*
E′f	15(317)	391 [40]	330	0.055	7	0.8	0.3	13,13	*b*
E′g	6(339)	408 [40]	350	0.003	25	1.2	0.1	20,30	2.5

[a] Maxima of single-photon absorption ($\lambda_E^{(1)}$) and molar absorption coefficients for single-photon absorption at $\lambda_E^{(1)}$, $\epsilon_E(\lambda_E^{(1)})$ (±5%) of the (*E*)-cinnamates; wavelength maxima ($\lambda_F^{(1)}$) and quantum yields ($\Phi_F^{(1)}$ ±10%) of fluorescence emission of the coumarin coproducts upon uncaging after one-photon excitation; excitation wavelength used for the series of uncaging experiments with one-photon excitation, $\lambda_{exc}^{(1)}$, relative brightness of the starting (*E*)-cinnamate with regard to brightness of the **F** coumarin coproduct at $\lambda_{exc}^{(1)}$, Q_E/Q_F, quantum yield of (*E*) to (*Z*) photoisomerization after one-photon excitation at $\lambda_{exc}^{(1)}$, $\Phi_{EZ}^{(1)}$ (±10%), action cross section for (*E*) to (*Z*) photoisomerization with one-photon excitation at $\lambda_{exc}^{(1)}$, $\epsilon_E(\lambda_{exc}^{(1)})\Phi_{EZ}^{(1)}$ (±5%), steady-state constant $K_1(\lambda_{exc}^{(1)}) = k_1(\lambda_{exc}^{(1)})/k_{-1}(\lambda_{exc}^{(1)})$ (±5%) associated to the **E** to **ZI** exchange with one-photon excitation at $\lambda_{exc}^{(1)}$, rate constant for the thermal (*Z*)-cinnamate to coumarin lactonization extracted from continuous illumination (k_2) and relaxation ($\not{k}_2$) experiments respectively (±10%), and action cross section for (*E*) to (*Z*) photoisomerization with two-photon excitation at $\lambda_{exc}^{(2)}$ =750 nm, $\delta_E(750)\,\Phi_{EZ}^{(2)}$ (±20%; GM, 1 GM = 10^{-50} cm^4 s (photon)$^{-1}$) for the (*E*)-cinnamate. Except for $\delta_E(750)\,\Phi_{EZ}^{(2)}$ given in acetonitrile, acetonitrile/Tris (pH = 7) 20 mM NaCl 100 mM buffer 1/1 (v/v) is the solvent. T = 293 K (see text and Supporting Information). [b] Not evaluated. [c] Too low to be reliably evaluated.

around their wavelength of maximum absorption, and the absorption and steady-state emission spectra were recorded after different illumination durations. The results are given in Table 1S in the Supporting Information. The main conclusions of this preliminary screening are the following: (i) The uncaging behavior is robust. All the **E′a**−**h** cinnamates release alcohol together with a strongly fluorescent coumarin coproduct upon one-photon illumination. Noticeably **E′h** exhibit a limited or very slow photoisomerization. (ii) Except for **E′e** in which the steric hindrance introduced by the 6-methoxy substituent probably forbids the phenyl conjugation with the double bond, the members of the **E′** series exhibit a significant absorption with one-photon excitation in the 300−400 nm wavelength range. Taking into account their donor−acceptor conjugated structure, the latter feature makes the series potentially appropriate to observe significant absorptions with two-photon excitation between 700 and 900 nm; (iii) **E′c** and **E′d** are not thermally stable (see Supporting Information). At room temperature, they isomerize in a few hours and thermally release the ethanol and the coumarin coproduct.

In fact, the latter preliminary observations made with the **E′** compounds led us to design the second **E** series of cinnamates displayed in Chart 2. We first removed the methyl group on the double bond to increase the energy barrier for thermal isomerization (see Supporting Information for a theorical schematic picture to analyze thermal and photochemical isomerization in the cinnamate series). Then we adopted the phenyl substituents leading both to significant absorptions beyond 300 nm and to fast enough uncaging.

After this preliminary screening, we eventually retained Tris (pH = 7) 20 mM NaCl 100 mM buffer/acetonitrile 1/1 (v/v) as a common solvent for one-photon experiments and **Ea**−**i**, **E′a**−**b**, **E′d**, **E′f**, and **E′g** as caged substrates for the following series of thorough investigations with one-photon excitation.

One-Photon Absorption of the Cinnamates. The absorption properties with one-photon excitation of the investigated (*E*)-cinnamates have been obtained by recording their UV−vis absorption spectra. In Tris (pH = 7) 20 mM NaCl 100 mM buffer/acetonitrile 1/1 (v/v), the investigated **E** and **E′** cinnamates exhibit an absorption spectrum in the 300−400 nm range. In the case of the less donating phenyl substituents (**a** and **b** derivatives), two bands are visible in the corresponding wavelength range (Figure 1S; see Supporting Information). In contrast, one notices the presence of a main band with a shoulder on its blue edge for the more electron-releasing phenyl substituents (see Figure 1). In all the investigated cases, the band at the lowest wavelength is the weakest among the two absorption bands. Noticeably, the position of the band associated to the more energetic transition is only weakly dependent on the substituent nature. In contrast, the band at the longest wavelength is red-shifted upon increasing the electron donating power of the phenyl substituent. Table 1 summarizes the absorption features, $\lambda_E^{(1)}$ and $\epsilon_E(\lambda_E^{(1)})$, associated to the band at the longest wavelength of the investigated (*E*)-cinnamates.

For a same phenyl substituent (entries **a**, **b**, and **d**), the absorption maximum with one-photon excitation $\lambda_E^{(1)}$ of the **E** derivative is systematically red-shifted by 14 kJ mol^{-1} (12−16 nm) compared to the one of the corresponding **E′**. This behavior is most probably related to a partial loss of planarity associated to a weaker conjugation in the **E′** series that would result from the steric hindrance between the methyl double-bond substituent and the *o*-hydroxy phenyl substituent.

As anticipated, $\lambda_E^{(1)}$ shifts to the red when the donating power of the conjugated phenyl substituent increases in both **E** and **E′** series. Hence, the longest maximal wavelength of absorption was observed for the julolidine derivative **Ei** ($\lambda_{Ee}^{(1)}$ = 394 nm) for which the absorption band significantly extends up to 450 nm. One should here notice the discrepancy between the nonbrominated **Ea** and dibrominated **Ec** 4-phenol cinnamates. In fact, the electron withdrawing properties of the bromine atoms in **Ec** decrease the protonation constant of its 4-hydroxy group by about 5 orders of magnitude (see Supporting Information). As a consequence, **Ec** is ionized at pH = 7 which gives rise to a phenoxy double bond substituent that is

Scheme 2. Mechanism of the Uncaging Process Leading to the Release of the Caged Alcohol **A** (Here Ethanol) Together with a Coumarin **F** When a Solution of (*E*) *o*-Hydroxycinnamate **E** Is Illuminated with One-Photon Excitation (Inspired from Schmir et al.)[22]

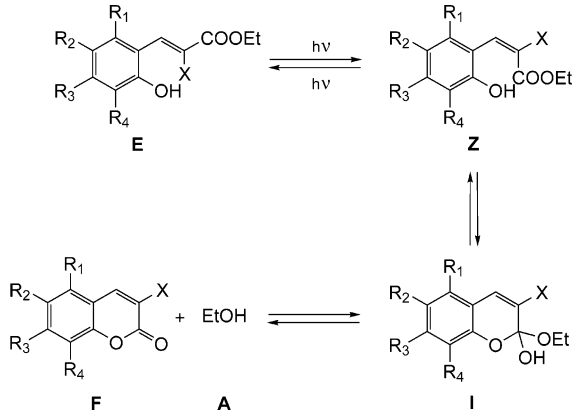

significantly more electron-donating than the corresponding phenol in **Ea**.

Eventually, the molar absorption coefficients at the wavelength of maximal absorption are satisfactorily large. Except for the naphthalene derivative **E′g**, $\epsilon_E(\lambda_E^{(1)}) \approx 2\ 10^4\ M^{-1}\ cm^{-1}$.

Irradiation Experiments with One-Photon Excitation. The irradiation experiments with one-photon excitation were performed stepwise.

In a first series of experiments, we used ^{1}H NMR and UV−vis absorption spectroscopy to analyze the species resulting from illumination of the caged (*E*)-cinnamates **E** and **E′** (see Supporting Information). In the case of **Ec**, we first showed that the uncaging process obeys the reaction displayed in Figure 1: The caged alcohol **A** (here ethanol) is released in a one-to-one stoichiometry together with a coumarin coproduct **F** upon illumination with one-photon excitation. This behavior is in line with Porter's previous observation.[14,26] Noticeably the (*E*)-cinnamates **E** and the corresponding coumarin **F** exhibit similar absorption properties making it possible to perform uncaging and excitation of the reporting fluorescent molecule with a same excitation source.

During this series of ^{1}H NMR experiments, we also identified an intermediate containing a double bond exhibiting a (*Z*) stereochemistry during the course of the photoconversion. Such an observation is in line with the previous observations of Schmir on a series of closely related coumarinic acids.[22,23] **Z** would be the primary intermediate that results from (*E*) to (*Z*) photoisomerization of the starting (*E*)-cinnamates (Scheme 2). A second intermediate **I** would be subsequently obtained from the nucleophilic addition of the *o*-hydroxy group onto the ethyl ester moiety.

We then turned to analyze the kinetics of the uncaging process in the present (*E*)-cinnamate series. Noticing that only the (*E*)-to-(*Z*) and (*Z*)-to-(*E*) cinnamate exchanges should be photochemically activated upon excitation at a large enough wavelength, we considered retrieving the photochemical properties of the present caging groups by analyzing their uncaging kinetics.

Figure 2a displays the typical temporal evolutions of the fluorescence emission from a solution of a (*E*)-cinnamate that is continuously illuminated at different light intensities at a wavelength $\lambda_{exc}^{(1)}$ closely located to its maximal wavelength of absorption $\lambda_E^{(1)}$. One can observe a large increase of fluorescence emission as a function of time that gets faster when the illumination intensity is increased.

The analysis of the curves displayed in Figure 2a requires a modeling of the uncaging process. In principle, Scheme 2 suggests consideration of a three step−six reactions mechanism that would involve six rate constants (Scheme 3a). However, it is possible to reduce the mechanism to a two step−three reactions mechanism (see Scheme 3b).

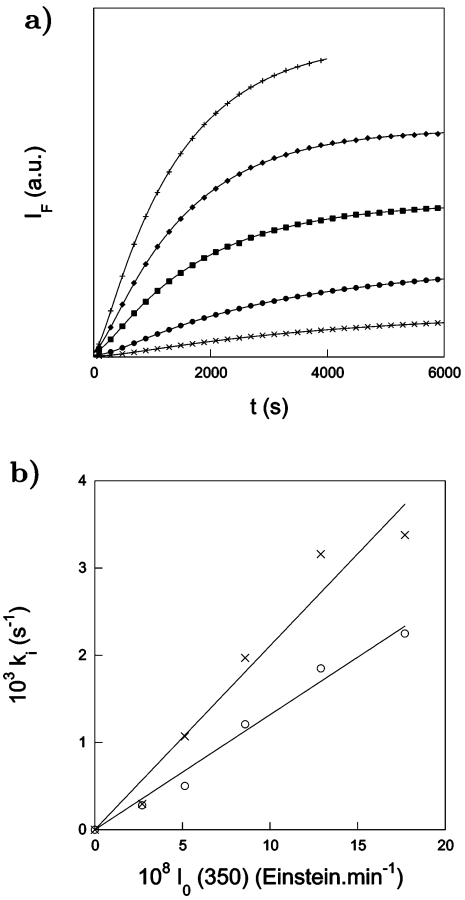

Figure 2. (a) Temporal evolution of the fluorescence emission at λ_{em} = 450 nm from a 5.7 μM **Ec** solution in acetonitrile/Tris (pH = 7) 20 mM NaCl 100 mM buffer 1/1 (v/v) upon one-photon irradiation ($\lambda_{exc}^{(1)}$ = 350 nm) at several incident light intensities $I_0(350)$ (from bottom to top in 10^{-8} Einstein min^{-1}: 2.7, crosses; 5.1, disks; 8.6, squares; 12.9, diamonds; 17.7, pluses). Markers indicate the experimental data; lines indicate fits with eq 14. (b) Dependence on the incident light intensities $I_0(350)$ of the rate constants k_1 (circles) and k_{-1} (crosses) extracted from the evolutions displayed in Figure 2a. T = 293 K (see Experimental Section).

Scheme 3. Reduction of the Mechanism of the Photochemical Isomerization of the (*E*)-Cinnamate **E** Leading to the Simultaneous Release of the Caged Alcohol **A** and of the Coumarin **F**

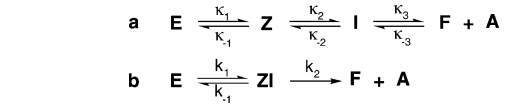

[a] Complete mechanism corresponding to the reactive scheme displayed in Scheme 2. The rate constants associated to each elementary step are denoted κ_i, where the subscript i indicates the corresponding step. [b] Reduced mechanism after taking into account the relative values of κ_2, κ_{-2}, κ_3, and κ_{-3}. The rate constants associated to each step of the reduced mechanism are denoted k_i, where the subscript i indicates the corresponding step.

(26) Porter, N. A.; Bruhnke, J. D. *J. Am. Chem. Soc.* **1989**, *111*, 7616−7618.

Taking advantage of the similar electronic demands of the hydroxy and ethoxy groups, we first relied on the thorough investigation of the cyclization of para substituted derivatives of coumarinic acid yielding the corresponding coumarins.[22,23] In the preceding work, the conversion of the **I**-type tetrahedral intermediate to the **F** coumarin with water release was reported to be the rate-limiting step of the **Z**-like coumarinic acid to the coumarin conversion in the case of coumarinic acids para substituted with electron donating conjugated substituents and at neutral pH like in the present study. Thus **Z** and **I** are suggested to be in fast exchange at the time scale of the **I** to **F** cyclization. At the same time, the rate constants associated to the photochemical exchange between the **E** and **Z** states and the rate constant for the **I** to **F** cyclization were in a comparable range under the present illumination conditions suggesting a consideration of **Z** and **I** in a fast exchange regime during the whole uncaging process. Eventually the final coumarin **F** is thermodynamically strongly favored among the different states displayed in Scheme 2 [22,23] so as to neglect the backward reaction from the coumarin **F** to the **I** intermediate in the final model. After introducing the **ZI** species that is relevant in describing **Z** + **I** when **Z** and **I** are in a fast exchange, we eventually retained the reduced model that is displayed in Scheme 3b to analyze the data.

The fit of data such as displayed in Figure 2a provides the values of the rate constants k_1, k_{-1}, and k_2 (see Experimental Section). Figure 2b shows that k_1 and k_{-1} depend linearly on the incident light intensity: this supports the model adopted in Scheme 3b. To bring further support to the model, we performed a complementary series of experiments to independently access the value of the rate constant k_2 by observing by UV−vis absorption spectroscopy the relaxation of solutions of the (*E*)-cinnamates after a short illumination with a UV lamp of large power; under such experimental conditions, only the **ZI** to **F** conversion of Scheme 3b is assayable. As displayed in Table 1, we obtained a satisfactory agreement between the k_2 values extracted from both series of experiments.

After the preceding model validation, we derived the photochemical properties of the *o*-hydroxycinnamate photolabile protecting group with one-photon excitation from k_1 and k_{-1} (see Experimental Section). k_1 gives the action (*E*) to (*Z*) photoisomerization cross section with one-photon excitation of the (*E*)-cinnamate **E**. The analysis of k_{-1} is more difficult because the equilibrium constant $\mathscr{K}_2$ associated to the fast exchange between **Z** and **I** cannot be measured which forbids us to derive the action (*Z*) to (*E*) photoisomerization cross section with one-photon excitation of the (*Z*)-cinnamate **Z**. The fit also yields the relative brightness of the starting (*E*)-cinnamate **E** with regards to the one of the coumarin coproduct **F**. Table 1 summarizes the results of the different parameters extracted from the series of irradiation experiments with one-photon excitation performed in the whole investigated **E** and **E′** series. The evidenced trends are examined and discussed in the following paragraphs.

Brightness of the (*E*)- and (*Z*)-Cinnamates and of the Coumarin Uncaging Coproducts. The release of a strongly fluorescent molecule compared to the initial caged molecule would be of great interest in quantifying the uncaging reaction in environments where reaction calibrations can prove to be daunting, such as in biological applications. Table 1 shows that the *o*-hydroxycinnamic series is especially favorable from this point of view: The brightness of the (*E*)-cinnamate caged compounds at the excitation wavelength required for uncaging is uniformly very low whereas the one of the coumarin coproduct is large. In fact, the emission from the starting cinnamate can be typically neglected in front of the one of the coumarin photoproduct beyond 1% extent of the uncaging process.

Quantum Yield of Photoisomerizations Involved in Uncaging. The quantum yields of (*E*)- to (*Z*)-cinnamate photoisomerization leading to alcohol uncaging are significant in both the **E** and **E′** series. They are always larger than 1% and reach up to 25% for **E′g**; in fact, they seem to be slightly larger in the **E′** series than in the **E** one (see Supporting Information for an interpretation). In particular, our 10% result for **E′d** satisfactorily compares with the 13% value reported by Porter et al. in Tris buffer.[27] Such values are in the range of the quantum yields associated to other relevant uncaging photochemistries. Lower values are generally observed for the most popular *o*-nitro benzyl photoisomerization,[28] whereas similar values are reported in the case of the coumaryl photolabile protecting group.[3]

Upon one-photon illumination, one does not only observe the (*E*)- to (*Z*)- but also the corresponding (*Z*)- to (*E*)-cinnamate photoisomerization in the present investigated series. In fact, the apparent thermodynamic constant $K_1 = k_1/k_{-1}$ which describes the exchange between the starting cinnamate **E** and the intermediate **ZI** is always lower than one except for **E′c** (Table 1). Such a result has been already observed by Porter et al. for the **E′d** derivative.[27] As anticipated from eq 17, K_1 depends on the excitation wavelength and peak at 0.6 at 375 nm (see Supporting Information). This behavior can be accounted for by the difference of the absorption spectra of the (*E*)- and (*Z*)-cinnamate as suggested from studying an ortho methoxy analogue of **Ec**, **EcMe** (see Supporting Information).

Rate Constant for the Thermally Driven Events Leading to Uncaging. Both series of experiments devoted to measure the rate constant k_2 associated to the thermal cyclization of the (*Z*)-cinnamates leading to alcohol release together with the formation of the corresponding coumarin coproduct provide similar values (Table 1). In the buffer−acetonitrile 1:1 (v:v) mixture, they lie in the 10^{-2} s^{-1} range for all the investigated compounds and are about 1 order of magnitude larger in the **E′** series than in the **E** one. One may additionally notice a trend for increasing the rate constant k_2 upon increasing the donating power of the phenyl para substituent in the **E** series.

The preceding observations are in line with the behavior observed in the coumarinic series for which the **I** to **F** reaction is the rate-limiting step during the thermal **Z** to **F** conversion at neutral pH (Scheme 2).[22,23] Indeed, the presence of the methyl substituent on the double bond is expected to accelerate the **I** to **F** reaction by increasing the associated release of steric hindrance with regards to the corresponding hydrogen derivative. In addition, the presence of an electron donating conjugated substituent in para of the phenyl group is expected to facilitate the release of the leaving-alcohol moiety.

(27) Koenigs, P. M.; Faust, B. C.; Porter, N. A. *J. Am. Chem. Soc.* **1993**, *115*, 9371−9379.
(28) Aujard, I.; Benbrahim, C.; Gouget, M.; Ruel, O.; Baudin, J. B.; Neveu, P.; Jullien, L. *Chem.−Eur. J.* **2006**, *12*, 6865−6879.

In fact, the k_2 value is expected to strongly depend on the nature of the caged substrate as well as on the solvent. Indeed, the rate limiting **I** → **F** step probably obeys here an E_1 mechanism associated to the loss of the alcohol moiety.[22] Then one anticipates k_2 to increase either with an increase of the withdrawal electronic properties of the alcohol or with an increase of the solvent polarity. During the present work, we did not attempt to modify the nature of the caged alcohol. Nevertheless it is here interesting to notice that Porter mentioned that the thermal cyclization of a (*Z*)-cinnamate to the corresponding coumarin occurred in less than 1 ms in the case of a phenol protected with an *o*-hydroxycinnamate moiety.[14] In contrast, we benefited from the favorable solubility properties of the **Ec** cinnamate to reproduce uncaging experiments in different solvents. We found the same $k_2 = 11\ 10^{-3}\ s^{-1}$ value in pure acetonitrile and in the acetonitrile/Tris (pH = 7) 20 mM NaCl 100 mM buffer 1/1 (v/v) mixture. In contrast, we observed a spectacular 300-fold increase of the corresponding rate constant in Tris (pH = 7) 20 mM NaCl 100 mM buffer: we found $k_2 = 0.3\ s^{-1}$. The latter results are in line with Porter's previous k_2 measurements for **E′d** in mixtures of ethanol and pH 7.4 Tris buffer in different proportions.[26] In particular, Porter found that k_2 varied by more than 3 orders of magnitude when going from ethanol/buffer 98:2 (v/v) ($k_2 = 7\ 10^{-4}\ s^{-1}$) to ethanol/buffer 2:98 (v/v) ($k_2 = 2\ s^{-1}$).

Irradiation Experiments with Two-Photon Excitation. In Vitro Uncaging. We took advantage of the release upon uncaging of the fluorescent coumarin in a one-to-one stoichiometry with the caged alcohol to measure the uncaging action cross section.

We first characterized the uncaging process by evidencing the photoinduced formation of the coumarin coproduct by means of its photophysical properties that can be investigated even at low concentrations. Figure 3a displays the temporal evolution of the fluorescence emission from a 1.8 μM **Ec** solution in acetonitrile upon irradiation at 750 nm at two laser powers.[29] One observes a continuous increase. Such a behavior is in line with the formation of a photoproduct that is more fluorescent than the starting (*E*)-cinnamate ester **Ec**. In a preceding communication,[9] we relied on a spectral analysis to conclude that this photoproduct was the coumarin **Fc**: both species exhibit the same emission spectrum with two-photon excitation. Fluorescence correlation spectroscopy (FCS) measurements also lead to the same conclusion (Figure 3b). Indeed the fluorophore that is formed upon illumination with two-photon excitation exhibits the same diffusion coefficient and flux of emitted photons per molecule and per second as the reference coumarin **Fc**.

Then we analyzed the kinetics of the uncaging process. In reference to the kinetic model displayed in Scheme 3b, the rate constant k_2 is now much larger than the rate constants k_1 and k_{-1} in the present conditions of illumination with two-photon excitation. Indeed the illuminated volume is lower with two- than with one-photon excitation during in vitro experiments (see eqs 15, 16, 18). Then only k_1 is here accessible: the Experimental Section explains that k_1 and the action cross section for

(29) To study uncaging with two-photon excitation for the whole series of cinnamates in a same solvent, we had to switch from the acetonitrile/buffer 1:1 (v/v) mixture to pure acetonitrile. Indeed, we observed in the former solvent that the fluorescence traces such as in Figure 3a periodically exhibited plateaus for the most hydrophobic derivatives (noticeably except for **Ec** which is fairly water-soluble).

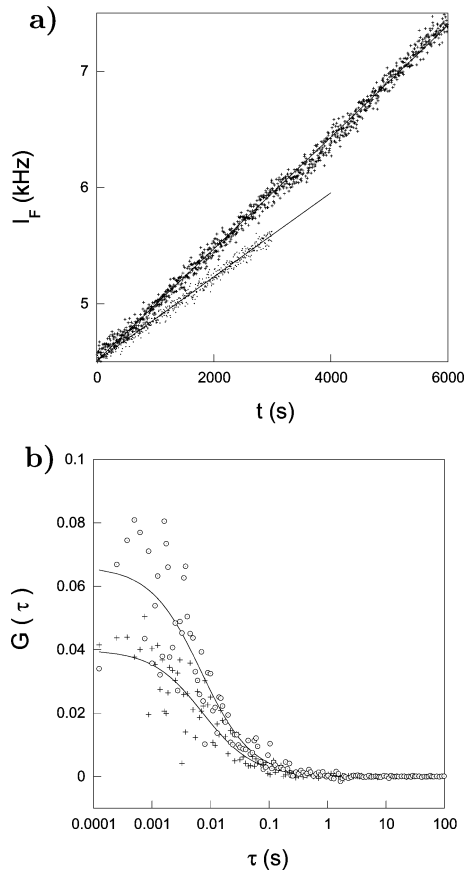

Figure 3. (a) Temporal evolution of the fluorescence emission from a 1.8 μM **Ec** solution in acetonitrile upon irradiation at $\lambda_{exc}^{(2)} = 750$ nm at two laser powers *P* (mW), 1.5 (dots) and 1.7 (pluses). The initial value of the two traces were made identical to favor the comparison of the slopes (see Experimental Section). (b) FCS autocorrelation curves $G(\tau)$ with two-photon excitation from the illuminated volume V_{exc} resulting from focusing the Ti−Sapphire laser beam at $P = 1.7$ mW after different illumination times: 0−1500 (circles) and 4500−6000 (pluses) s. Fitting (solid line) of the experimental points (markers) with eq 2, respectively provided 7 ± 3 μs and 7 ± 3 μs for the diffusion time τ_D and 15 and 25 for the number of fluorescent molecules contained within the excitation volume V_{exc}. After taking into account the intensity of fluorescence emission from V_{exc} that was measured at the APD, we evaluate at 300 Hz the flux of emitted photons per fluorescent molecule and per second that satisfactorily compared with the value measured for the reference **Fc** coumarin. The data shown in Figure 3a and 3b are used to extract the action (*E*) to (*Z*) photoisomerization cross section with two-photon excitation at $\lambda_{exc}^{(2)} = 750$ nm, $\delta_E(750)\ \Phi_{EZ}^{(2)}$: solvent, acetonitrile; $T = 293$ K.

(*E*)- to (*Z*)-cinnamate photoisomerization with two-photon excitation can be extracted from the slope of the linear temporal evolution of the fluorescence intensity displayed in Figure 3a. In particular, we verified in the course of this series of experiments that the dependence of the rate constant k_1 with the average laser power was quadratic so as to conclude that the observed behavior did result from two-photon absorption.

Table 1 displays the (*E*) to (*Z*) photoisomerization action cross sections with two-photon excitation of several (*E*)-cinnamates at $\lambda_{exc}^{(2)} = 750$ nm in acetonitrile. They are all 1 order of magnitude larger than the 0.1 GM limit which was claimed to be the lowest value relevant for biological applications.[3] In fact, the **Ee** value equal to 4.7 GM at 750 nm is the largest reported to date.[3]

In Vivo Uncaging. Having quantitatively characterized in vitro the behavior of a caged alcohol, we were willing to investigate whether the *o*-hydroxycinnamic moiety would be

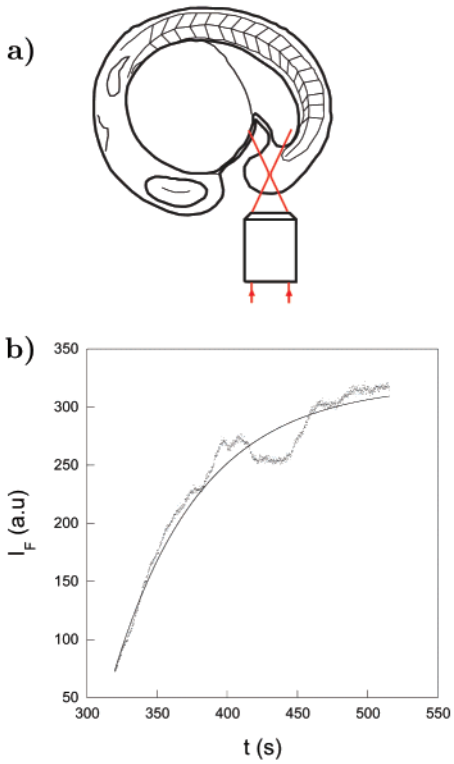

Figure 4. Evaluation of two-photon uncaging with fluorescence reporting of the *o*-hydroxycinnamic platform in vivo (a zebrafish embryo is used for illustration). The embryo was incubated in a 10 μM aqueous solution of nonfluorescent caged alcohol **Ec** that penetrates in the whole organism. The embryo was subsequently submitted to a continuous two-photon excitation by focusing a laser beam (red arrows) in the caudal fin area (a) and the fluorescence signal emitted from the illuminated tiny zone was recorded as a function of time. The uncaging process is specifically revealed by the exponential dependence on time of singular fluorescence rises observed along the fluorescence trace (b) (see text and Experimental Section).

appropriate as a photolabile protecting group for biological applications in a living organism. We adopted the zebrafish animal model that seems particularly promising for the use of light to control biological activity: its embryo is transparent, unpigmented strains are available, and it has recently emerged as an attractive model animal for numerous studies.[30]

We first incubated a zebrafish embryo at the 10−15 somite stage in a 10 μM solution of **Ec** for 60 min. We subsequently illuminated at 750 nm the caudal fin area (Figure 4a) and we continuously recorded the fluorescence emission arising from the focal point. We observed a smooth increase of the fluorescence signal (see Figure 4b). Ethanol uncaging occurred in the illuminated cell releasing the fluorescent coumarin coproduct **Fc** characterized from its emission spectrum:[9] Thus we concluded that two-photon uncaging with fluorescence reporting is active at the single-cell level in vivo in the *o*-hydroxycinnamic series.

It can be shown that the temporal dependence of the fluorescence emission during uncaging in a closed volume is exponential if the starting cinnamate **Ec** and the coumarin photoproduct **Fc** do not permeate at the uncaging time scale (see Supporting Information). Such an exponential behavior was indeed observed by analyzing individual fluorescence rises such as shown in Figure 4b. The final asymptotic value associated to the exponential fit of the fluorescence emission from the focal spot was in line with the signal intensity expected from the coumarin **Fc** in aqueous solution at a typical 10 μM concentration. We further checked the agreement between the plateau value and the incubating solution concentration by conducting the same experiment with a more dilute solution (500 nM) and recorded the FCS autocorrelation curve upon uncaging completion. We measured a 500 nM **Fc** concentration inside cells (see eq 2 in Experimental Section). Such observations suggest that the initial intracellular concentration in caged precursor **Ec** was essentially similar to the concentration of the incubating solution.

The rate given by the exponential fit is the one of the limiting step in the uncaging reaction. We measured 6×10^{-3} s^{-1}. The expected rate from a 1.6 GM uncaging action cross section with two-photon excitation of **Ec** at 750 nm[9] would be 20 s^{-1} at 4.5 mW power in this closed environment (see eq 18 in Experimental Section and data not shown). This value is 3 orders of magnitude greater than the measured rate. We thus can rule out the (*E*)-to-(*Z*) photoisomerization of **Ec** as limiting step. A first possible rate-limiting step could be here the **ZIc** to **Fc** conversion. Indeed, we do not know what is actually the location of the (*E*)-cinnamate **Ec** within an embryo cell, and we observed that k_2 is considerably decreased if **Ec** is not located in water but in an organic-like medium. Another possible explanation could be that the uncaging process is limited by the off-rate constant of some complex involving **Ec** that would be located out from the laser focal point. In both cases, it is here important to notice that the observed uncaging rate constant would considerably depend on the structure of the caged alcohol.

Discussion

Evaluating the efficiency of a caging group is a complex issue. Indeed the demands on the caging group can vary considerably depending on the application. In the following discussion, we are essentially concerned with discussing two aspects of the *o*-hydroxycinnamic platform for uncaging applications in biology. We first examine processing issues that are relevant to condition the biological sample. We subsequently discuss the uncaging opportunities provided by the *o*-hydroxycinnamic photolabile moiety for two-photon uncaging in a biological context.

During this study, we have been particularly concerned with the solubility of the caged substrate. This point is especially significant for biological applications. For instance, in the zebrafish embryo considered here, the caged substrate has first to be dissolved in an aqueous solution, which requires an exhibition of some hydrophilicity, and then reach the targeted cell, which involves crossing hydrophobic barriers. From the latter point of view, the *o*-hydroxycinnamic platform is particularly favorable: this photolabile moiety is synthetically easily accessible, and the different substituents on the benzene ring can be easily changed to finely tune the hydrophilic/hydrophobic balance in the caged derivatives as well as in the coumarin coproduct. In particular, we consider as satisfactory the results obtained with **Ec** (and **Fc**) in which we introduced in the *o*-hydroxycinnamic caging moiety a conjugated acidic phenol with a protonation constant in the range of intracellular pH (4.5−7.5). First, the native acidic state absorbs only rather far in the UV: the strong UV−vis absorption yielding uncaging only occurs after dissolution in water, and the pure caged substrate

(30) Zon, L. I.; Peterson, R. T. *Nat. Rev. Drug Discovery* **2005**, *4*, 35−44.

can be easily stored as an inert compound. Furthermore, at neutral pH such as in a cell, the caged substrate constantly switches between its acidic uncharged phenol state (making it soluble in a lipophilic environment such as a bilayer) and its basic negatively charged phenate form (conferring water solubility). Water solubility facilitates organism exposition to the caged substrate and the dual hydrophilic/hydrophobic character probably explains why we found **Ec** at the concentration of the incubating **Ec** solution even in cells deeply embedded in the zebrafish embryo. At the same time, the coumarin coproduct **Fc** is significantly water-soluble which permits a reliable interpretation of its fluorescence emission in vivo.[9]

Two-photon uncaging has been especially considered for biological applications in view of its promising spatial and temporal resolution. However most photochemically driven substrate releases involve a multistep mechanism with both photochemical and thermal reactions.[11] The primary photochemical event initiated at the focal spot of the laser beam and the subsequent substrate release are consequently most often decoupled in time and, correspondingly, in space since the intermediates generated after illumination would be generally free to diffuse. Thus a detailed kinetic analysis not restricted to the photochemical events is required to appreciate the efficiency of a photolabile protecting group for given two-photon uncaging applications.[7,31] In the two following paragraphs, we examine two generic situations according to the position of the focal spot with regard to the cellular environment.

In extracellular photolysis, uncaging occurs in a volume which can be considered as infinite and two-photon uncaging is used to generate in the focal spot a concentration in photoreleased substrate that significantly departs from its concentration in the environment. Then an "efficient'' caging group has to exhibit rate constants associated to the primary photochemical event as well as to the subsequent thermal reactions larger than the rate of diffusion through the laser beam waist (typically 10^4 s^{-1}).[31,32] Moreover increasing the latter rate constants beyond the diffusion rate still improves the uncaging efficiency. To have a tunable delivery at nondetrimental laser powers, the rate-limiting step should be the primary photochemical event in which a two-photon uncaging action cross section should be at least be equal to 0.1−1 GM at 750 nm.

The boundary conditions are very different in intracellular photolysis: Two-photon uncaging now occurs in a closed volume and one is concerned with generating a homogeneous intracellular concentration in released substrate from a caged precursor faster than the biological phenomena to be triggered. The lower temporal resolution is now fixed by an homogenization time which is at least in the 10−100 ms range for a typical "small'' substrate in a 1000 μm^3 cell.[33] Then an "efficient'' caging group only requires the rate constants of the primary photochemical event and of the subsequent thermal reactions to be larger than the rate of diffusion within the closed territory (typically 10^1−10^2 s^{-1}). Noticeably increasing the preceding rate constant does not improve here the uncaging efficiency but only forces diffusion to be taken into account to yield the intracellular distribution in photoreleased substrate. In fact, the constraint on the rate constant in the case of intracellular photolysis is rather permissive in terms of action cross section with two-photon excitation of the primary photochemical event: 1 mGM range is now sufficient to be "efficient'' at nondetrimental laser powers.

In the present *o*-hydroxycinnamate system, the primary photochemical event is the (*E*)- to (*Z*)-cinnamate photoisomerization which is associated to action cross sections with two-photon excitation exceeding the 1 GM range. From the latter point of view, the *o*-hydroxycinnamate is an excellent photochemical platform belonging to the most efficient available to date.[3,5,8] Nevertheless, one has also to take into account the thermal reactions involved in the substrate release. Although Porter reported rate constants larger than 10^3 s^{-1} for phenol uncaging, we here observed at most the 1 s^{-1} range for alkyl alcohol uncaging with **Ec** in water. To increase the latter value, the present study suggests some possible improvement associated with modifying the substitution pattern of the cinnamate double bond: For instance, we observed that the addition of a methyl substituent increased k_2 by a factor of ten. At the present time, we estimate that the *o*-hydroxycinnamate system should be essentially restricted for alcohol uncaging in intracellular photolysis where its excellent fluorescence reporting features are particularly appropriate to yield information on the amount of released substrate. As an example, it should prove to be useful to control gene expression through the release of ligands for transcription factors. Indeed, tetracyclin and ecdysone are the inducers of two widely used gene expression inducible systems;[34,35] they contain alcohol groups which can be used to graft *o*-hydroxycinnamate groups to inactivate their biological functions. Moreover, the relevant biological timescales associated with gene expression are fully compatible with release rates in the 1 s^{-1} or even the 10^{-2} s^{-1} range.

Conclusion

The present investigation underlines the significance of the *o*-hydroxycinnamic platform to design versatile photolabile protecting groups with fluorescence reporting for alcohols upon one- and two-photon excitation. The *o*-hydroxycinnamate series is synthetically easily accessible. An appropriate choice of the different substituents on the benzene ring is expected to allow for fine-tuning of the hydrophilic/hydrophobic balance in the caged derivatives as well as in the coumarin coproduct upon alcohol uncaging. In addition, the robust photophysical and photochemical properties are particularly attractive. The maximal wavelength for one-photon absorption of the *o*-hydroxycinnamates can be easily tuned at the UV−vis limit where the cinnamates exhibit a strong absorption. The caged alcohol is essentially nonfluorescent and quantitatively releases upon one-photon excitation the alcohol substrate together with a strongly fluorescent coumarin coproduct in a one-to-one molar ratio. Uncaging and excitation of the reporting fluorescent molecule can be additionally done using the same excitation source. We eventually observed maximal wavelength and action cross sections associated to uncaging upon two-photon excitation that favorably compare with the best reported values.

(31) Brown, E. B.; Shear, J. B.; Adams, S. R.; Tsien, R. Y.; Webb, W. W. *Biophys. J.* **1999**, 76, 489−499.
(32) Kiskin, N. I.; Ogden, D. *Eur. Biophys. J.* **2002**, 30, 571−587.
(33) In fact, one should also consider here that a caged compound might form a complex with some intracellular components (bilayer, proteins) not located at the laser focus. Then the apparent homogeneization time could be associated to the off-rate of the caged substrate from the complex.
(34) Cambridge, S. B.; Geissler, D.; Keller, S.; Curten, B. *Angew. Chem., Int. Ed.* **2006**, *45*, 2229−2231.
(35) Lin, W.; Albanese, C.; Pestell, R. G.; Lawrence, D. S. *Chem. Biol.* **2002**, *12*, 1347−1353.

The *o*-hydroxycinnamic caging group appears particularly attractive in biological applications that do require precise but not necessarily "fast'' two-photon excitation-induced substrate release. In particular, our results suggest that quantitative control of substrate delivery could be achieved in vivo at the second time scale by recording the fluorescence emission from the coumarin **F** coproduct that reports on the concentration in photoreleased substrate.

Experimental Section

Syntheses. 2,4-Dihydroxybenzaldehyde, 2-hydroxy-4-methoxybenzaldehyde, 4-diethylamino-2-hydroxybenzaldehyde, 2-hydroxy-5-nitrobenzaldehyde, 2-hydroxy-4,6-dimethoxybenzaldehyde, carboethoxyethylidenetriphenylphosphorane and carboethoxymethylidenetriphenylphosphorane were commercially available. The syntheses of the other starting substituted benzaldehydes and of the 1-carboxymethylidene triphenylphosphorane are reported in Supporting Information.

General Procedures. The commercially available chemicals were used without further purification. Anhydrous solvents were freshly distilled before use. Column chromatography (CC) used silica gel 60 (0.040−0.063 mm) from Merck; analytical and thin layer chromatography (TLC) was performed with Merck silica gel 60 F_{254} precoated plates, detection by UV (254 nm); melting point used a Büchi 510. ^{1}H NMR and ^{13}C NMR spectra were obtained by AM 250 SY Bruker. Chemical shifts (δ) in ppm related to protonated solvent as internal reference: (^{1}H) $CHCl_3$ in $CDCl_3$, 7.26 ppm; CHD_2COCD_3 in CD_3COCD_3, 2.20 ppm; CHD_2SOCD_3 in CD_3SOCD_3, 2.54 ppm; (^{13}C) $^{13}CDCl_3$ in $CDCl_3$, 77.0 ppm; $^{13}CD_3COCD_3$ in CD_3COCD_3, 29.8 ppm; $^{13}CD_3SOCD_3$ in CD_3SOCD_3, 39.6 ppm. Coupling constants *J* are given in Hz. Mass spectrometry (chemical ionization and high resolution with NH_3 or CH_4) was performed at the Service de Spectrométrie de masse de l'ENS. Microanalyses were obtained from the Service de Microanalyses de l'Université Pierre et Marie Curie, Paris.

General Procedure for Wittig Reactions.[25] A mixture of aldehyde and carboethoxyethylidenetriphenylphosphorane or carboethoxymethylidenetriphenylphosphorane (1.5 equiv) in toluene (10 mL for 1 mmol of aldehyde) was heated at 60 °C under argon upon protecting from light. The course of the reaction was followed by TLC (cyclohexane/AcOEt). After 2 to 4 h, the reaction was completed. After cooling to room temperature, toluene was removed in a vacuum. The crude residue was purified by flash chromatography on silica gel (mixtures of ethyl acetate and cyclohexane as eluent) to yield the desired cinnamate in high yield (from 60 to 90%; about 10% of the coumarin resulting from thermal trans−cis isomerization followed by lactonization was formed during the reaction).

(*E*)-3-(2,4-Dihydroxyphenyl)-2-methyl Acrylic Acid Ethyl Ester (E′a). Yield. 60%; mp 121−122 °C. ^{1}H NMR (ppm, 250 MHz, CD_3COCD_3, 298 K) δ: 8.63 (bs, 1 H), 7.9 (s, 1 H), 7.27 (d, 1 H, J = 8.4 Hz), 6.5 (d, 1 H, J = 2.3 Hz), 6.45 (dd, 1 H, J = 8.4 Hz, J = 2.3 Hz), 4.22 (q, 2 H, J = 7 Hz), 2.07 (s, 3 H), 1.31 (t, 3 H, J = 7 Hz). ^{13}C NMR (ppm, 62.8 MHz, CD_3COCD_3, 298 K) δ: 168.6, 159.7, 157.7, 134.5, 131.5, 125.1, 115.2, 107.3, 102.9, 60.3, 14.1, 14.0. Anal. Calcd (%) for $C_{12}H_{14}O_4$ (222.09): C, 64.85; H, 6.35. Found: C, 64.63; H, 6.31. Mass spectrometry, MS (CI, NH_3): *m*/*z* 223 [M + 1].

(*E*)-3-(6-Hydroxy-benzo(1,3)dioxo-5-yl)-2-methyl Acrylic Acid Ethyl Ester (E′b). Yield, 70%; mp 113−114 °C. ^{1}H NMR (ppm, 250 MHz, $CDCl_3$, 298 K) δ: 7.65 (s, 1 H), 6.70 (s, 1 H), 6.47 (s, 1 H), 5.94 (s, 1 H), 5.02 (s, 2 H) 4.27 (q, 2 H, J = 7.1 Hz), 2.02 (s, 3 H), 1.34 (t, 3 H, J = 7.1 Hz). ^{13}C NMR (ppm, 62.8 MHz, CD_3COCD_3, 298 K) δ: 168.9, 125.5, 149.7, 141.6, 135.0, 126.5, 115.7, 109.3, 102.3, 98.6, 61.0, 14.7, 14.5. Anal. Calcd (%) for $C_{13}H_{14}O_5$ (250): C, 62.39; H, 5.64. Found: C, 62.27; H, 5.59. Mass spectrometry, MS (CI, CH_4): *m*/*z* 251 [M + 1]. MS (CI, CH_4, HR): *m*/*z* 251.0924 (calcd mass for $C_{13}H_{15}O_5$, 251.0919).

(*E*)-3-(3,5-Dibromo-2,4-dihydroxy-phenyl)-2-methyl Acrylic Acid Ethyl Ester (E′c). Yield, 35%; mp 112−114 °C. H NMR (ppm, 250 MHz, $CDCl_3$, 298 K) δ: 7.67 (s, 1 H), 7.38 (s, 1 H), 5.99 (s, 1 H), 5.88 (s, 1 H), 4.27 (q, 2 H, J = 7.1 Hz), 2.03 (d, 3 H, J = 1.4 Hz), 1.34 (t, 3 H, J = 7.2 Hz). C NMR (ppm, 62.8 MHz, $CDCl_3$, 298 K) δ: 168.2, 151.1, 149.7, 132.0, 131.3, 129.7, 117.4, 100.1, 99.0, 61.0, 14.2 (2C). Anal. Calcd (%) for $C_{12}H_{12}O_4Br_2$ (380.03): C, 37.93; H, 3.18. Found: C, 37.70; H, 3.10. Mass spectrometry, MS (CI, CH_4): *m*/*z* 381 [M + 1]. MS (CI, CH_4, HR): *m*/*z* 380.9161 (calcd mass for $C_{12}H_{13}O_4{}^{79}Br^{81}Br$, 380.9153).

(*E*)-3-(4-Diethylamino-2-hydroxy-phenyl)-2-methyl Acrylic Acid Ethyl Ester (E′d).[25] Yield, 70%; mp 96−97 °C. H NMR (ppm, 250 MHz, $CDCl_3$, 298 K) δ: 7.71 (s, 1 H), 7.12 (d, 1 H, J = 8.2 Hz), 6.21 (dd, 1 H, J_1 =8.7 Hz, J_2 =2.4 Hz), 6.1 (d, 1 H, J = 2.4 Hz), 5.3 (s, 1 H), 4.18 (q, 2 H, J = 7.1 Hz), 3.27 (q, 4 H, J = 7.1 Hz), 2.01 (s, 3 H), 1.26 (t, 3 H, J = 7.17 Hz), 1.1 (t, 6 H, J = 7.1 Hz). ^{13}C NMR (ppm, 62.8 MHz, $CDCl_3$, 298 K) δ 169.3, 155.6, 149.6, 133.6, 131.2, 125.1, 110.2, 104.3, 98.0, 60.7, 44.4 (2C), 14.4 (2C), 12.7 (2C). Anal. Calcd (%) for $C_{16}H_{23}O_3N$ (277.36): C, 69.28; N, 5.05; H, 3.18. Found: C, 69.14; N, 5.07; H, 8.65. Mass spectrometry, MS (CI, CH_4): *m*/*z* 278 [M + 1]. MS (CI, CH_4, HR): *m*/*z* 278.1761 (calcd mass for $C_{16}H_{24}O_3N$, 278.1756).

(*E*)-3-(2-Hydroxy-4,6-dimethoxy-phenyl)-2-methyl Acrylic Acid Ethyl Ester (E′e). Yield, 30%; mp 99 °C. ^{1}H NMR (ppm, 250 MHz, $CDCl_3$, 298 K) δ: 7.49 (d, 1 H, J = 1.1 Hz), 6.12 (dd, 2 H, J =2.1 Hz, J =1.1 Hz), 4.93 (s, 1 H), 4.27 (q, 2 H, J = 7.1 Hz), 3.79 (s, 3 H), 3.78 (s, 3 H), 1.57 (s, 3 H), 1.34 (t, 3 H, J = 7.1 Hz). ^{13}C NMR (ppm, 62.8 MHz, $CDCl_3$, 298 K) δ: 168.1, 161.8, 158.8, 154.5, 131.5, 131.3, 104.6, 93.2, 91.3, 60.9, 55.6, 55.4, 15.0, 14.3. Anal. Calcd (%) for $C_{14}H_{18}O_5$ (266.12): C, 63.15; H, 6.81. Found : C, 63.14; H, 6.72. Mass spectrometry, MS (CI, NH_3): *m*/*z* 367 [M + 1].

(*E*)-3-(2-Hydroxy-4-methoxyphenyl)-2-methyl Acrylic Acid Ethyl Ester (E′f). Yield, 60%; mp 99 °C. ^{1}H NMR (ppm, 250 MHz, $CDCl_3$, 298 K) δ: 7.73 (s, 1 H), 7.11 (d, 1 H, J = 9.2 Hz), 6.8 (bs, 1 H), 6.42 (s, 1 H), 6.39 (d, 1 H, J = 9.2 Hz), 4.17 (q, 2 H, J = 7.2 Hz), 3.68 (s, 3 H), 1.96 (s, 3 H), 1.24 (t, 3 H, J = 7.1 Hz). ^{13}C NMR (ppm, 62.8 MHz, $CDCl_3$, 298 K) δ: 169.4, 161.1, 155.7, 134.2, 130.8, 127.4, 115.7, 106.1, 101.5, 61.0, 55.2, 14.2, 14.1. Anal. Calcd (%) for $C_{13}H_{16}O_4$ (236.10): C, 66.09; H, 6.83. Found: C, 66.03; H, 6.78. Mass spectrometry, MS (CI, NH_3): *m*/*z* 237 [M + 1].

(*E*)-3-(2-Hydroxy-naphtalen-1-yl)-2-methyl Acrylic Acid Ethyl Ester (E′g). Yield, 80%; mp 94−96 °C. ^{1}H NMR (ppm, 250 MHz, $CDCl_3$, 298 K) δ: 7.9 (s, 1 H), 7.7 (m, 3 H), 7.47−7.21 (m, 3 H), 5.6 (bs, H), 4.35 (q, 2 H, J = 7.0 Hz), 1.87 (d, 3 H, J = 0.9 Hz), 1.40 (t, 3 H, J = 7.3 Hz). ^{13}C NMR (ppm, 62.8 MHz, $CDCl_3$, 298 K) δ: 167.6, 150.0, 134.5, 132.8, 132.1, 130.2, 128.7, 128.3, 126.8, 123.9, 123.7, 117.6, 114.6, 61.2, 14.6, 14.3. Anal. Calcd (%) for $C_{16}H_{16}O_3$ (256): C, 75.00; H, 6.25. Found: C, 74.95; H, 6.28. Mass spectrometry, MS (CI, CH_4): *m*/*z* 257 [M + 1]. MS (CI, CH_4, HR): *m*/*z* 257.1176 (calcd mass for $C_{16}H_{17}O_3$, 257.1178).

(*E*)-3-(2-Hydroxy-5-nitrophenyl)-2-methyl Acrylic Acid Ethyl Ester (E′h). Yield, 50%; mp 115−115.5 °C. ^{1}H NMR (ppm, 250 MHz, $CDCl_3$, 298 K) δ: 8.15 (m, 2 H), 7.63 (s, 1 H), 6.99 (d, 1 H, J = 9.2 Hz), 6.10 (s, 1 H), 4.31 (q, 2 H, J = 7.1 Hz), 2.03 (d, 3 H, J = 1.2 Hz), 1.37 (t, 3 H, J = 7.2 Hz). ^{13}C NMR (ppm, 62.8 MHz, $CDCl_3$, 298 K) δ: 169.1, 160.1, 140.9, 132.4, 131.9, 126.1, 125.9, 123.3, 116.1, 61.8, 14.2 (2C). Anal. Calcd (%) for $C_{12}H_{13}NO_5$ (251): C, 57.37; N, 5.58; H, 5.22. Found: C, 57.45; N, 6.58; H, 5.30. Mass spectrometry, MS (CI, CH_4): *m*/*z* 252 [M + 1].

(*E*)-3-(2,4-Dihydroxyphenyl) Acrylic Acid Ethyl Ester (Ea). Yield, 70%; mp 193−195 °C. ^{1}H NMR (ppm, 250 MHz, CD_3SOCD_3, 298 K) δ: 10.12 (bs, 1 H), 9.9 (bs, 1 H), 7.78 (d, 1 H, J = 16 Hz), 7.42 (d, 1 H, J = 8.6 Hz), 6.4−6.35 (m, 2 H), 6.28 (dd, 1 H, J = 8.4 Hz, J = 2.1 Hz), 4.15 (q, 2 H, J = 7.2 Hz), 1.24 (t, 3 H, J = 7.2 Hz). ^{13}C NMR (ppm, 62.8 MHz, CD_3SOCD_3, 298 K) δ: 167.1, 160.9, 158.5,

140.3, 130.3, 113.0, 112.6, 107.8, 102.4, 59.4, 14.3. Anal. Calcd (%) for $C_{11}H_{12}O_4$ (208.07): C, 63.45; H, 5.81. Found: C, 63.37; H, 5.80.

(*E*)-3-(6-Hydroxy-benzo(1,3)dioxo-5-yl) Acrylic Acid Ethyl Ester (Eb). Yield, 60%; mp 149−150 °C. ^{1}H NMR (ppm, 250 MHz, $CDCl_3$, 298 K) δ: 8.02 (d, 1 H, $J = 16.1$ Hz), 6.92 (s, 1 H), 6.41 (s, 1 H), 6.31 (d, 1 H, $J = 15.9$ Hz), 6.02 (s, 1 H) 5.95 (s, 2 H), 4.26 (q, 2 H, $J = 7.1$ Hz), 1.29 (t, 3 H, $J = 7.1$ Hz). ^{13}C NMR (ppm, 62.8 MHz, CD_3-$COCD_3$, 298 K) δ: 167.8, 153.7, 151.5, 142.6, 140.1, 115.5, 114.7, 106.5, 102.5, 98.6, 60.4, 14.7. Anal. Calcd (%) for $C_{12}H_{12}O_5$ (236): C, 61.01; H, 5.12. Found: C, 60.86; H, 5.21. Mass spectroscopy, MS (CI, CH_4): *m*/*z* 237 [*M*+1]. MS (CI, CH_4, HR): *m*/*z* 237.0762 (calcd mass for $C_{12}H_{13}O_5$, 237.0763).

(*E*)-3-(3,5-Dibromo-2,4-dihydroxyphenyl) Acrylic Acid Ethyl Ester (Ec). Yield, 40%; mp 118−118.5 °C. ^{1}H NMR (ppm, 250 MHz, $CDCl_3$, 298 K) δ: 7.81 (d, 1 H, $J = 16.1$ Hz), 7.60 (s, 1 H), 6.47 (d, 1 H, $J = 16.1$ Hz), 6.07 (bs, 2 H), 4.22 (q, 2 H, $J = 7.0$ Hz), 1.33 (t, 3 H, $J = 7.0$ Hz). ^{13}C NMR (ppm, 62.8 MHz, CD_3COCD_3, 298 K) δ: 167.3, 154.2, 153.7, 138.7, 131.6, 118.8, 117.8, 102.1, 101.8, 60.7, 14.6. Anal. Calcd (%) for $C_{11}H_{10}O_4Br_2$ (365.9): C, 36.10; H, 2.75. Found: C, 36.06; H, 2.63. Mass spectrometry, MS (CI, CH_4): *m*/*z* 367 [$M + 1$]. MS (CI, CH_4, HR): *m*/*z* 364.9024, 366.9006, and 368.8992 (calcd mass for $C_{11}H_{10}O_4Br_2$: 364.9024, 366.9004, and 368.8985).

(*E*)-3-(4-Diethylamino-2-hydroxy-phenyl) Acrylic Acid Ethyl Ester (Ed). Yield, 65%; mp 134−137 °C. ^{1}H NMR (ppm, 250 MHz, $CDCl_3$, 298 K) δ: 7.88 (d, 1 H, $J = 15.9$ Hz), 7.31 (d, 1 H, $J = 8.8$ Hz), 6.33 (d, 1 H, $J = 15.9$ Hz), 6.25 (d, 1 H, $J = 8.8$ Hz), 6.03 (s, 1 H), 5.66 (s, 1 H), 4.24 (q, 2 H, $J = 7.1$ Hz), 3.34 (q, 4 H, $J = 7.0$ Hz), 1.32 (t, 3 H, $J = 7.0$ Hz), 1.16 (t, 6 H, $J = 7.0$ Hz). ^{13}C NMR (ppm, 62.8 MHz, $CDCl_3$, 298 K) δ: 168.6, 156.8, 150.7, 140.3, 130.7, 112.2, 110.0, 105.1, 98.0, 60.0, 44.5 (2C), 14.4, 12.6 (2C). Anal. Calcd (%) for $C_{15}H_{21}O_3N$ (263.3): C, 68.40; H, 8.03; N, 5.31. Found: C, 67.87; H, 7.98; N, 5.65. Mass spectroscopy, MS (CI, CH_4): *m*/*z* 264 [$M +$ 1]. MS (CI, CH_4, HR): *m*/*z* 264.1596 (calcd mass for $C_{15}H_{22}O_3N$: 264.1600).

(*E*)-3-(8-Hydroxy-2,3,6,7-tetrahydro-1*H*,5*H*-pyrido(3,2,1-ij)quinolin-9-yl) Acrylic Acid Ethyl Ester (Ei). Yield, 75%; mp 167−169 °C. ^{1}H NMR (ppm, 250 MHz, $CDCl_3$, 298 K) δ: 7.86 (d, 1 H, $J = 15.8$ Hz), 6.97 (s, 1 H), 6.24 (d, 1 H, $J = 15.8$ Hz), 4.95 (s, 1 H), 4.22 (q, 2 H, $J = 7.1$ Hz), 3.38 (q, 4 H, $J = 5.2$ Hz), 2.67 (t, 4 H, $J = 6.4$ Hz), 1.94 (m, 4 H), 1.31 (t, 3 H, $J = 7.0$ Hz). ^{13}C NMR (ppm, 62.8 MHz, CD_3 OCD_3, 298 K) δ: 168.4, 153.8, 146.7, 141.5, 126.5, 115.2, 111.5, 111.0, 108.0, 59.9, 50.6, 49.8, 28.0, 22.8, 22.1, 22.0, 14.8. Anal. Calcd (%) for $C_{17}H_{21}O_3N$ (287): C, 71.06; N, 4.87; H, 7.37. Found: C, 70.83; N, 4.70; H, 7.5. Mass spectroscopy, MS (CI, CH_4): *m*/*z* 288 [$M + 1$]. MS (CI, CH_4, HR): *m*/*z* 288.1603 (calcd mass for $C_{17}H_{22}O_3N$: 288.1600).

Solutions. Except for pK_a measurements performed in the Britton−Robinson buffer[36] (acetic acid, boric acid, phosphoric acid) at 0.1 M, in vitro experiments were made in CH_3CN/20 mM Tris (pH = 7) 100 mM NaCl buffer 1/1 v/v or in acetonitrile. No thermal (*E*) to (*Z*) isomerization or thermal ester hydrolysis were ever observed at the time scale of the present experiments (24 h).

pH Measurements. pH measurements were performed on a Standard pH meter PHM210 Radiometer Analytical that was calibrated with buffers at pH 4 and 7.

Spectroscopic Measurements and Irradiation Experiments. One-Photon Excitation. UV−Visible Absorption. UV/vis absorption spectra were recorded at 293 K on a Kontron Uvikon-940 spectrophotometer. Molar absorption coefficients were extracted while checking the validity of the Beer−Lambert law.

The evolutions of the absorbance as a function of pH were analyzed with the *SPECFIT/32* Global Analysis System (version 3.0 for 32-bit Windows systems) to extract the pK_a of the ground state (see Supporting Information).[37]

Steady-State Fluorescence Emission. Corrected fluorescence spectra upon one-photon excitation were obtained from a Photon Technology International LPS 220 spectrofluorimeter. Solutions for fluorescence measurements were adjusted to concentrations such that the absorption maximum was around 0.15 at the excitation wavelength. The overall fluorescence quantum yields after one-photon excitation $\Phi_F^{(1)}$ were calculated from the relation (1):

$$\Phi_F^{(1)} = \Phi_{ref}^{(1)} \frac{1 - 10^{-A_{ref}(\lambda_{exc})}}{1 - 10^{-A(\lambda_{exc})}} \frac{D}{D_{ref}} \left(\frac{n}{n_{ref}}\right)^2 \quad (1)$$

where the subscript ref stands for standard samples. $A(\lambda_{exc})$ is the absorbance at the excitation wavelength, *D* is the integrated emission spectrum, and *n* is the refractive index for the solvent. The uncertainty in the experimental value of $\Phi_F^{(1)}$ was estimated to be ±10% . The standard fluorophore for the quantum yields measurements was quinine sulfate in 0.1 M H_2SO_4 with $\Phi_{ref}^{(1)} = 0.55$.[38]

Irradiation Experiments. Three different protocols have been used to perform the irradiations relying on one-photon excitation.

The experiments devoted to the identification of the products from the photochemical isomerization of the cinnamate **Ec** by ^{1}H NMR were performed for various durations at 20 °C by putting a bench top UV lamp (6 W 365 nm UV lamp; Fisher Bioblock) above a cuvette containing $V = 2.5$ mL of illuminated solution that was subsequently transferred into a NMR tube.

The experiments devoted to evidencing the formation of the coumarin **Fc** from the photochemical isomerization of the cinnamate **Ec** by UV−vis absorption as well as to analyze the kinetics of **E** photoisomerization were performed on 2.5 mL samples in 1 × 1 cm^2 quartz cuvettes under constant stirring. Excitations were performed with the 75 W xenon lamp of a Photon Technology International LPS 220 spectrofluorometer. In the case of the kinetics experiments, the continuous illumination was performed at several slit widths to cover a significant range of incident light intensities. The corresponding incident light intensities were systematically calibrated by determining the kinetics of photoconversion of the α-(4-dimethylaminophenyl)-*N*-phenylnitrone into 3-(4-dimethylaminophenyl)-2-phenyloxaziridine in fresh dioxane as described in ref 39. During the present series of experiments, typical incident light intensities were in the 10^{-7} einstein min^{-1} range.

The experiments devoted to analyze the kinetics of the thermal processes following the (*E*) to (*Z*) cinnamate photoisomerization were performed on 2.5 mL samples in 1 × 1 cm^2 quartz cuvettes. The cuvette was continuously submitted to the irradiation from a bench top UV lamp (6 W 365 nm UV lamp; Fisher Bioblock) for 1 min. The absorbance was subsequently recorded as a function of time on the red edge of the absorption band.

Two-Photon Excitation. The two-photon experiments were performed with a home-built setup[9,40] using fluorescein for calibration. Illumination comes from a mode-locked titanium−sapphire laser (Mira pumped by Verdi, Coherent). Fluorescence photons were collected with an Olympus UPlanApo 60 × 1.2 NA water immersion objective through filters (AHF Analysentechnik) and optical fibers (FG200LCR multimode fiber, Thorlabs) connected to two avalanche photodiodes (SPCM-AQR-14, Perkin-Elmer, Vaudreuil, Canada) coupled to an ALV-6000 correlator (ALV GmbH). The excitation input power was measured with a Lasermate powermeter (Coherent) or a Nova II

(36) Frugoni, C. *Gazz. Chim. Ital.* **1957**, *87*, 403−407.

(37) Gampp, H.; Maeder, M.; Meyer, C. J.; Zuberbühler, A. D. *Talanta* **1985**, *32*, 95−101. Gampp, H.; Maeder, M.; Meyer, C. J.; Zuberbühler, A. D. *Talanta* **1985**, *32*, 257−264. Gampp, H.; Maeder, M.; Meyer, C. J.; Zuberbühler, A. D. *Talanta* **1985**, *32*, 1133−1139. Gampp, H.; Maeder, M.; Meyer, C. J.; Zuberbühler, A. D. *Talanta* **1986**, *33*, 943−951.

(38) Demas, J. N.; Crosby, G. A. *J. Phys. Chem.* **1971**, *75*, 991−1024.

(39) Wang, P. F.; Jullien, L.; Valeur, B.; Filhol, J. S.; Canceill, J.; Lehn, J. M. *New J. Chem.* **1996**, *20*, 895−907.

(40) Charier, S.; Meglio, A.; Alcor, D.; Cogné-Laage, E.; Allemand, J. F.; Jullien, L.; Lemarchand, A. *J. Am. Chem. Soc.* **2005**, *127*, 15491−15505.

powermeter (Ophir Optronics Ltd.). Powers were kept under 5 mW at the sample to stay in the quadratic range for absorption and to be not detrimental to cells in the in vivo application.[41] The intensity and the temporal correlation function of the collected fluorescence emission are recorded.

FCS Experiments. FCS autocorrelation curve $G(\tau)$ were recorded during the irradiation experiments devoted to extract the action photoisomerization cross sections with two-photon excitation (vide infra). At the beginning of the irradiation experiment, the fluorescence emission from the solution of the cinnamate **E** is too weak to record any tractable FCS curve. Therefore we first irradiate the **E** solution to produce enough coumarin coproduct **F** to get enough signal and appropriate FCS curves: We typically excite the solution at 750 nm with a laser power in the 1−2 mW range for $\Delta t_0 = 2$ h which typically corresponds to 1% of $\mathbf{E} \rightarrow \mathbf{F}$ photoconversion. Beyond Δt_0, any FCS autocorrelation curve $G(\tau)$ can be reliably fitted by assuming that the solution contains one freely diffusing species only: the coumarin **F**. Indeed, the contribution of the residual caged alcohol **E** in the $G(\tau)$ curve can be neglected owing to the weak **E** brightness. We consequently used eq 2 to fit the experimental FCS autocorrelation curves $G(\tau)$ displayed in Figure 3b:[42]

$$G(\tau) = \frac{1}{N_F}\frac{1}{1+\tau/\tau_D} \tag{2}$$

In eq 2, N_F and τ_D designate the average number of **F** molecules in the illuminated spot described as 2D-Gaussian and the diffusion time of **F** through the beam waist.

Irradiation Experiments. The irradiations were performed on 2.5 μL samples contained in a cylindrical well made of parrafin (radius, 1.25 mm; height, 2 mm) sealed with Parafilm (no evaporation occurs on a time scale of several days).

Kinetic Analysis of the Photoisomerization of the Cinnamates E to the Coumarins F. The Model. We are here interested in the derivation of the theoretical expressions of the concentrations in **E**, **Z**, **I**, and **F** (E, Z, I, and F, respectively) during the in vitro uncaging process.

We first assume that the system (volume V) is homogeneous at any time of its evolution. In fact, the whole system is not homogeneously illuminated during the irradiation experiments; only part of the system (volume V_{exc}) is submitted to light. Thus matter transport has to be considered to support the homogeneity assumption:

(1) In the case of the one-photon illumination, the cuvette content is continuously stirred, and the homogeneity assumption is fulfilled as soon as uncaging does not occur much below the second time scale which is here the case.

(2) In contrast, there is no such stirring upon two-photon illumination; homogeneization is controlled by diffusion. In fact, we take here again advantage from the slow uncaging rates with regards to the homogeneization process: the uncaging relaxation time is much larger than the characteristic time τ_V required for **E**, **Z**, **I**, and **F** to diffuse in the whole system. Indeed, for in vitro two-photon experiments, $V = 2.5$ μL and $\tau_V = 4$ min, whereas $\tau_u = 1/(k_1 + k_{-1}) \simeq 4700$ min in the fastest situations encountered during that work.

Thus the following equations can be considered as valid beyond a characteristic homogeneization time scale by considering concentrations averaged over the whole volume V.

Then we rely on the mechanism displayed in Scheme 3a to write eqs (3−6) describing the concentration evolutions:

$$\frac{dE}{dt} = -\kappa_1 E + \kappa_{-1} Z \tag{3}$$

$$\frac{dZ}{dt} = \kappa_1 E - (\kappa_{-1} + \kappa_2) Z + \kappa_{-2} I \tag{4}$$

$$\frac{dI}{dt} = \kappa_2 Z - (\kappa_{-2} + \kappa_3) I + \kappa_{-3} F \times A \tag{5}$$

$$\frac{dF}{dt} = \kappa_3 I - \kappa_{-3} F \times A \tag{6}$$

where A designates the concentration in photoreleased alcohol.

Then we first take into account that the exchange between **Z** and **I** is fast at the time scale of the in vitro irradiation experiments; beyond the relaxation time associated to the $\mathbf{Z} \rightleftarrows \mathbf{I}$ exchange, it is meaningful to introduce the average species **ZI** (concentration $ZI = Z + I$; then the concentrations in **Z** and **I** are $(1/(1+\mathscr{K}_2))$ ZI and $(\mathscr{K}_2/(1+\mathscr{K}_2))$ ZI, respectively, where $\mathscr{K}_2$ designates the equilibrium constant associated to the conversion of **Z** into **I**). We additionally consider the large coumarin stability to neglect the terms associated to the back reaction (−3) in eqs 5−6. Thus eqs 3−6 transform into eqs 7−9:

$$\frac{dE}{dt} = -k_1 E + k_{-1} ZI \tag{7}$$

$$\frac{dZI}{dt} = k_1 E - (k_{-1} + k_2) ZI \tag{8}$$

$$\frac{dF}{dt} = k_2 ZI \tag{9}$$

with $k_1 = \kappa_1$, $k_{-1} = (1/(1+\mathscr{K}_2))\kappa_{-1}$, and $k_2 = (\mathscr{K}_2/(1+\mathscr{K}_2))\kappa_3$. Equations 7−9 make clear the interpretation of the reduced mechanism displayed in Scheme 3b, that it is only valid beyond the time scale for exchange between **Z** and **I**.

During the continuous illumination experiments, the differential equation governing the temporal evolution of F is

$$\frac{d^3F}{dt^3} + (k_1 + k_{-1} + k_2)\frac{d^2F}{dt^2} + k_1 k_2 \frac{dF}{dt} = 0 \tag{10}$$

Considering that the system initially only contains **E** (initial concentration E_0), we get after integration:

$$E = \frac{E_0}{\sqrt{\Delta}}\left(\frac{\sqrt{\Delta}+k_1}{2} e^{(-(k_1+k_{-1}+k_2+\sqrt{\Delta})t/2)} + \frac{\sqrt{\Delta}-k_1}{2} e^{(-(k_1+k_{-1}+k_2-\sqrt{\Delta})t/2)}\right) \tag{11}$$

$$ZI = \frac{k_1 E_0}{\sqrt{\Delta}}\left(e^{(-(k_1+k_{-1}+k_2-\sqrt{\Delta})t/2)} - e^{(-(k_1+k_{-1}+k_2+\sqrt{\Delta})t/2)}\right) \tag{12}$$

$$F = \frac{2k_1 k_2 E_0}{\sqrt{\Delta}}\left[\frac{1}{k_1+k_{-1}+k_2+\sqrt{\Delta}}(-1 + e^{(-(k_1+k_{-1}+k_2+\sqrt{\Delta})t/2)}) + \frac{1}{k_1+k_{-1}+k_2-\sqrt{\Delta}}(1 - e^{(-(k_1+k_{-1}+k_2-\sqrt{\Delta})t/2)})\right] \tag{13}$$

where $\Delta = (k_1 + k_{-1} + k_2)^2 - 4k_1 k_2$.

(41) During the present series of experiments, we observed the formation of holes from focusing the laser beam in the zebrafish embryo at laser powers beyond 15 mW at 750 nm at the sample. We do not think that this detrimental effect results from heat associated with light absorption with residual one-photon excitation at 750 nm followed by nonradiative deexcitation. First, below 5 mW at 750 nm at the sample, water does not lead to any significant heating (see: Schönle, A.; Hell, S. W.; *Opt. Lett.* **1998**, *23*, 325−327). In addition, the zebrafish embryo does not contain any significant amount of interfering endogeneous chromophores at that step of development. In particular, we were never able to express GFP under control of a heat-shock promoter by simply focusing the IR laser beam in any targeted cell of an appropriate transgenic embryo. In fact, we estimate that our observation is more probably related to plasma formation that occurs at 10 mW at 750 nm even in pure solvents (see: Sacchi, C. A. *J. Opt. Soc. Am. B* **1991**, *8*, 337−345. Vogel, A.; Noack, J.; Hüttman, G.; Paltauf, G.; *App. Phys. B* **2005**, *85*, 1015−1047).

(42) Krichevsky, O.; Bonnet, G. *Rep. Prog. Phys.* **2002**, 65, 251−297.

Introducing $\mathscr{Q}_E$, $\mathscr{Q}_{ZI}$ and $\mathscr{Q}_F$ the brightnesses of **E**, **ZI**,[43] and **F**, respectively, we eventually derive the temporal evolution of the fluorescence intensity I_F as

$$I_F = \alpha\frac{E_0}{\sqrt{\Delta}}\left[\sqrt{\Delta}\mathscr{Q}_F + e^{(-(k_1+k_{-1}+k_2-\sqrt{\Delta})t/2)}\left(\mathscr{Q}_{ZI}k_1 + \mathscr{Q}_E\frac{\sqrt{\Delta}-k_1}{2} - \mathscr{Q}_F\frac{2k_1k_2}{k_1+k_{-1}+k_2-\sqrt{\Delta}}\right) + e^{(-(k_1+k_{-1}+k_2+\sqrt{\Delta})t/2)}\left(-\mathscr{Q}_{ZI}k_1 + \mathscr{Q}_E\frac{\sqrt{\Delta}+k_1}{2} + \mathscr{Q}_F\frac{2k_1k_2}{k_1+k_{-1}+k_2+\sqrt{\Delta}}\right)\right] \quad (14)$$

where α is a collecting factor of fluorescence emission.

In the case of relaxation experiments devoted to independently measuring the rate constant associated to the thermal conversion of **ZI** to **F**, the evolution of the sample absorption with one-photon excitation $\mathscr{A}$ is followed as a function of time after an initial strong illumination pulse. Adopting the second step displayed in Scheme 3b to model the system relaxation, the absorbance $\mathscr{A}$ obeys an exponential law: $\mathscr{A}(t) = \mathscr{A}_0 \exp(-k_2t) + \mathscr{A}_\infty[1 - \exp(-k_2t)]$.

Extraction of the Action Photoisomerization Cross Sections with One- and Two-Photon Excitation. One-Photon Illumination. The orders of magnitude of k_1, k_{-1}, and k_2 are similar under the present experimental conditions with one-photon excitation. The fluorescence evolution is thus directly fitted with eq 14 using $\chi_1 = (k_1 + k_{-1} + k_2 - \sqrt{\Delta})/2$, $\chi_2 = (k_1 + k_{-1} + k_2 + \sqrt{\Delta})/2$, $A_1 = ((\mathscr{Q}_{ZI}/\mathscr{Q}_F)k_1 + \mathscr{Q}_E/\mathscr{Q}_F(\sqrt{\Delta} - k_1)/2 - k_1k_2/\chi_1)$ and $A_2 = (-(\mathscr{Q}_{ZI}/\mathscr{Q}_F)k_1 + \mathscr{Q}_E/\mathscr{Q}_F(\sqrt{\Delta} + k_1)/2) + k_1k_2/\chi_2)$ as floating parameters. k_1, k_{-1}, and k_2 are then extracted from analyzing the dependence of χ_1 and χ_2 on light intensity. In addition, A_1 and A_2 provide $\mathscr{Q}_{ZI}/\mathscr{Q}_F$ and $\mathscr{Q}_E/\mathscr{Q}_F$.

The action photoisomerization cross sections with one-photon excitation are eventually derived from the expressions of k_1 and k_{-1} given by the relations (15−16):[39]

$$k_1 = \frac{2.3\epsilon_E(\lambda_{exc}^{(1)})\phi_{EZ}^{(1)}l}{V}I_0(\lambda_{exc}^{(1)}) \quad (15)$$

$$k_{-1} = \frac{1}{1+\mathscr{K}_2}\frac{2.3\epsilon_Z(\lambda_{exc}^{(1)})\phi_{ZE}^{(1)}l}{V}I_0(\lambda_{exc}^{(1)}) \quad (16)$$

In eqs (15,16), $\epsilon_E(\lambda_{exc}^{(1)})$ and $\epsilon_Z(\lambda_{exc}^{(1)})$, $\phi_{EZ}^{(1)}$, and $\phi_{ZE}^{(1)}$, l, V, and $I_0(\lambda_{exc}^{(1)})$ designate the molar absorption coefficients of the (*E*) and (*Z*) cinnamate stereoisomers, the quantum yields for the (*E*)- to (*Z*)- and (*Z*)- to (*E*)-photoconversions, the path length of the light beam, the irradiated volume, and the light intensity at the excitation wavelength, respectively.

In Table 1, we introduce the steady-state constant $K_1(\lambda_{exc}^{(1)})$ associated to the **E** to **ZI** exchange with one-photon excitation at $\lambda_{exc}^{(1)}$:

$$K_1 = (1+\mathscr{K}_2)\frac{\epsilon_E(\lambda_{exc}^{(1)})\phi_{EZ}^{(1)}}{\epsilon_Z(\lambda_{exc}^{(1)})\phi_{ZE}^{(1)}} \quad (17)$$

Two-Photon Illumination. To derive the expressions of k_1 and k_{-1} when two-photon excitation is used, we consider that the reactions (1) and (−1) displayed in Scheme 3b take place only in the focal volume V_{exc} resulting from laser focusing. The value k_2 is now much larger than k_1 and k_{-1} under the present experimental conditions with two-photon excitation. In particular, $\chi_1 = k_1$ and $\chi_2 = k_2$ at first order. Upon assuming that the reservoir of starting cinnamate is infinite ($E = E_0$) and by neglecting the brightness of **E** in front of the one of **F**, one easily demonstrates that the temporal fluorescence evolution given in eq 14 becomes linear in the kinetic regime between the times $1/k_2$ and $1/k_1$ which was analyzed here. Then the corresponding slope of the linear I_F variation is equal to $\dot{I}_F = \alpha\mathscr{Q}_FE_0k_1$.

$\alpha\mathscr{Q}_F$ can be independently measured by recording and analyzing the APD counts and the autocorrelation curve from a solution of the coumarin **F**. The APD counts provide $\alpha\mathscr{Q}_FN_FP^2$ where N_F and P designate the average number of **F** molecules in the illuminated spot and the laser power at the sample. The FCS autocorrelation curve gives N_F from the ordinate at the origin, and P is measured with the powermeter.

E_0 being known, k_1 can be thus derived from $\dot{I}_F$.[44] The action photoisomerization cross section with two-photon excitation $\delta_E^{(2)}\Phi_{EZ}^{(2)}$ is eventually derived from the expressions of k_1 following Kiskin et al.:[7]

$$k_1 = 0.737\delta_E\Phi_{EZ}^{(2)}\mathscr{T}\tau_P\left(\frac{\lambda}{\pi hcw_{xy}^2}\right)^2\frac{V_{exc}}{V}P^2 \quad (18)$$

In eq 18, δ_E, $\Phi_{EZ}^{(2)}$, $\mathscr{T}$, τ_P, and w_{xy} designate the cross sections for two-photon absorption leading to (*E*)- to (*Z*)-photoisomerization at the excitation wavelength $\lambda_{exc}^{(2)}$ of **E**, the quantum yields associated to the (*E*)- to (*Z*)-photoconversions after two-photon excitation, the period of the laser pulses (13.6 ns in our case), the duration of the laser pulses (200 fs), and the waist of the focused laser beam (0.3 μm).

Acknowledgment. Prof. Sophie Vriz is gratefully acknowledged for generous gifts of zebrafish embryos. Dr. Jean-François Allemand is gratefully acknowledged for his help in designing FCS experiments. This research is financially supported by the "Association pour la Recherche sur le Cancer'' (ARC) (2005, Project n3787).

Supporting Information Available: Syntheses of the noncommercially available starting substituted benzaldehydes and of the 1-carboxymethyliden triphenyl phosphorane; preliminary screening of the thermal stability and the photophysical and the photochemical properties of the caged model compounds **E′a**−**h** in aqueous solutions (Table 1S); a schematic picture to analyze the photochemical and thermal isomerizations in the cinnamate series (Schemes 1S and 2S); UV−vis absorption spectra of **Ea** and **Eb** (Figure 1S); measurement of the **Ec** and **Fc** protonation constants (Figures 2Sa−c); identification of the products from the photochemical isomerization of the cinnamate **Ec** with one-photon excitation (Figures 3Sa−b, 4Sa−d, and 5S); dependence of the apparent thermodynamic constant for the **Ec** to **ZIc** exchange on the one-photon excitation wavelength (Figures 6S and 7S, Scheme 3S); model for the kinetics of two-photon uncaging in vivo. This material is available free of charge via the Internet at http://pubs.acs.org.

JA0722022

(43) $\mathscr{Q}_{ZI} = (1/(1+\mathscr{K}_2))\mathscr{Q}_Z + (\mathscr{K}_2/(1+\mathscr{K}_2))\mathscr{Q}_I$ where $\mathscr{Q}_Z$ and $\mathscr{Q}_I$ designate the brightnesses of **Z** and **I**, respectively.

(44) Although here less precise, a satisfactory order of magnitude of k_1 can also be extracted from the FCS data. In the considered kinetic regime, **E** can be considered to directly afford **F** with k_1 rate constant and the number of **F** molecules in the focal point, N_F, increases linearly with time with a slope E_0k_1. Then the average number of molecules $1/G(0) = <N_F>_{[t_1;t_2]}$ extracted from the FCS experiment between time t_1 and t_2 (0 and 1500 s, and then 4500 and 6000 s in the experiment shown in Figure 3b) is given by the expression:

$$\frac{1}{<N_F>_{[t_1;t_2]}} = \frac{1}{t_2-t_1}\int_{t_1}^{t_2}\frac{dt}{E_0k_1t+N_F^0} = \frac{1}{E_0k_1(t_2-t_1)}\ln\left(\frac{E_0k_1t_2+N_F^0}{E_0k_1t_1+N_F^0}\right)$$

where N_F^0 is the number of **F** molecules in the focal point a $t = 0$ s. Then the results from at least two FCS experiments provide $N_F{}^0$ and k_1. In the case of the curves displayed in Figure 3b, we can extract in particular $k_1 = 1.2 \times 10^{-6}$ s^{-1} which is in good agreement with the value obtained from the slope extracted from Figure 3a, $k_1 = 1.0 \times 10^{-6}$ s^{-1}.